Economic Geology, v. 104, pp. 905–944

Cordilleran Epithermal Cu-Zn-Pb-(Au-Ag) Mineralization in the Colquijirca District, Central Peru: Deposit-Scale Mineralogical Patterns

Ronner Bendezú[†,1,2] and Lluís Fontboté[2]

[1]*Bilbao 295, Lima, Peru*

[2]*Sciences de la Terre et de l'environnement, Université de Genève, Rue de Maraîchers 13, CH-1205, Genève, Switzerland*

Abstract

At Colquijirca, central Peru, a Miocene diatreme-dome complex is associated in space and time with several large epithermal polymetallic (Cu-Zn-Pb-Au-Ag) deposits of the Cordilleran class. Of these deposits, Smelter and Colquijirca, located in the northern sector of the district, are part of a continuously mineralized north-south corridor that extends for nearly 4 km outward from the diatreme-dome complex and to depths of 1 km below surface. This corridor is zoned from Cu-(Au) ores in its inner parts (Smelter deposit) to peripheral Zn-Pb-(Ag) ores (Colquijirca deposit). The Smelter-Colquijirca corridor has undergone minor erosion, providing a good example of a nearly intact paleo-epithermal system of the Cordilleran class.

This description of the hypogene mineralogical patterns of the Smelter-Colquijirca corridor leads to the proposal that they are the result of superimposition in time and space of three main stages. During an early quartz-pyrite stage, in which basically no economic ore deposition occurred, carbonate rocks surrounding the Marcapunta diatreme-dome complex were replaced by quartz and pyrite. This was followed by the main ore stage, which was largely superimposed on the quartz-pyrite replacements and produced zonation of ore minerals and metals along much of the Smelter-Colquijirca corridor. The zoning from Cu ores to Zn-Pb ores is complex and comprises a number of distinct and well-defined zones that display abrupt or gradual interfaces between zones. From internal to external parts, these zones consist mainly of the following mineral associations and assemblages: (1) enargite ± (luzonite, pyrite, colusite, tennantite, goldfieldite, ferberite, gold-silver tellurides, bismuthinite, gold, alunite, zunyite, kaolinite, dickite, smectite, illite, sericite, quartz); (2) enargite ± (pyrite, quartz, bismuthinite, alunite, dickite, kaolinite, smectite, illite, sericite); (3) bornite ± (pyrite, quartz, alunite, dickite, kaolinite, barite); (4) tennantite, barite ± (dickite, kaolinite, chalcopyrite, Bi- and/or Ag-bearing minerals); (5) chalcopyrite, sphalerite, galena ± (pyrite, quartz, dickite, kaolinite, barite); (6) sphalerite, galena, pyrite ± (hematite, kaolinite, siderite, magnetite, marcasite); (7) Zn-bearing carbonate zone; and (8) a barren outer zone consisting mainly of calcite. The crosscutting relationships and zoning patterns indicate that during the main ore stage, the inner Cu zones progressively overprinted the Zn-Pb zones. Evidence for the subsequent contraction of the mineralization front is also recognized. A mainly fault-controlled late ore stage was the last recognized episode of mineralization in the Smelter-Colquijirca corridor, related to the deposition of chalcocite, digenite, and covellite as veinlets cutting and replacing the different Cu-bearing zones of the main ore stage; it is not economically important.

The different mineral associations and assemblages provide insights into the chemistry of the hydrothermal fluids, particularly that of the main ore stage. The acidity and oxidation state of the main ore-stage fluids varied considerably prior to significant interaction with the host rock. This is best observed in the enargite-bearing zones in which most acidic fluids formed alunite-zunyite-enargite–bearing assemblages and less acidic fluids formed smectite-illite-enargite and muscovite-enargite–bearing assemblages. The common kaolinite-dickite-enargite assemblage was related to a fluid with intermediate character between these two end-member styles. The significant fluctuations in the acidity of the ore fluids in the central parts of the mineralizing system are interpreted to reflect mixing between variable amounts of acidic and oxidized magmatic vapor-derived fluids and less acidic low to moderate saline ore-forming fluids of magmatic origin.

Introduction

Peru is a major producer of silver, copper, zinc, lead, bismuth, tin, and gold. Of these metals, zinc, lead, silver, tin, and bismuth are produced dominantly from deposits of several styles but all sharing the following major features: (1) polymetallic (Cu-Zn-Pb-Ag-Au) suite; (2) zoned from inner Cu-bearing to outer Zn-Pb–bearing ores; (3) sulfide-rich character, commonly massive; and (4) primary occurrence as open-space fillings (veins, breccia bodies) in silicate host rocks and as replacements in carbonate rocks. Sawkins (1972) classified ores displaying these features as Cordilleran vein-type deposits. Later, Einaudi (1982) described these deposits as Cordilleran vein or lode deposits within the context of porphyry-related systems. Additional general discussions on Cordilleran vein deposits are given by Guilbert and Park (1986), Bartos (1989), and Fontboté and Bendezú (2009). Recently, this type of mineralization has been termed "zoned base metal veins" by Einaudi et al. (2003); however, a clear zonation is not always recognized, and the ores in many districts are dominantly mantos and not veins, and they commonly contain Au and Ag in addition to base metals. We therefore prefer the more general term "Cordilleran polymetallic deposits" (Bendezú et al., 2008; Fontboté and Bendezú, 2009).

Until the 1980s (Guilbert and Park, 1986), Cordilleran ores were not commonly recognized to be associated with porphyry-Cu deposits or their associated intrusive rocks. During

[†] Corresponding author: e-mail, Ronner.Bendezu@terrapristina.com

Submitted: September 16, 2009
Accepted: September 28, 2009

the last few decades, extensive mining and exploration in mature districts have revealed that these polymetallic ores are mainly located at shallower levels than the porphyry-Cu-(Au-Mo) and/or skarn mineralization centers (e.g., Quiruvilca, Noble and McKee, 1999; Yauricocha, Alvarez and Noble, 1988; Magma, Manske and Paul, 2002; Vinchos, Farfán, 2006; Morococha, Bendezú, 2007; Catchpole et al., 2008; Kouzmanov et al., 2008). Fluid inclusions studies in several Cordilleran deposits indicate that this ore type precipitated mostly under epithermal conditions (e.g., Colqui, Kamilli and Ohmoto, 1977; Hualgayoc, MacFarlane et al., 1990; San Cristobal, Beuchat et al., 2004; Colquijirca, Bendezú, 2007; Cerro de Pasco, Baumgartner et al., 2008).

In Peru, Cordilleran deposits are found only in the high Andes between 3,500 and 5,000 m above sea level (asl). Examples from northern and central Peru display a broad variety of mineral associations which form a continuum between the following two end-member styles:

1. Strongly zoned deposits consisting of cores dominated by enargite, pyrite, quartz ± (tennantite, wolframite, chalcopyrite, covellite, chalcocite, alunite, dickite, kaolinite) and external parts by sphalerite, galena ± (sericite, kaolinite, dickite, hematite, Mn-Fe carbonates). Examples include most of Smelter-Colquijirca, parts of Cerro de Pasco, Hualgayoc, Quiruvilca, Yauricocha, Morococha, San Cristobal, Huarón, and Julcani.
2. Weakly zoned deposits consisting of internal zones with (pyrrhotite), pyrite, quartz ± (chalcopyrite, arsenopyrite, tetrahedrite, carbonates, sericite, chlorite, quartz) and external zones with Fe-rich sphalerite, galena, pyrrhotite ± (Mn-Fe carbonates, sericite, chlorite, quartz). Examples include Malpaso, Huanzalá, Huagochugcho, Huaraucaca, Vinchos, and parts of Cerro de Pasco and Morococha.

Many Peruvian Cordilleran deposits display one of these contrasting mineral associations or intermediate associations in between, but in some cases, including Cerro de Pasco and Morococha, both end-member styles are present in the same deposit. In these two examples the mineral assemblages indicate that pH and sulfidation states of mineralizing fluids fluctuated, from strongly acidic and very high sulfidation states, to weakly acidic and low-sulfidation states, respectively.

The Colquijirca district, as well as the nearby Cerro de Pasco district, is related to one of the easternmost Miocene magmatic belts of central and northern Perú (~360 km from the Peruvian trench). The Colquijirca district is located at 4,300 m asl on the Meseta de Bombon high plateau of the central Peruvian Andes near 11°S and 76°W (Fig. 1). Two main types of epithermal mineralization occur in the district, both with close temporal and spatial relationships to the Marcapunta Miocene diatreme-dome volcanic complex (Fig. 1). These are the high-sulfidation Au-(Ag) ores emplaced within the Marcapunta diatreme-dome complex (Vidal et al., 1997; Bendezú et al., 2003), and the economically more important Cordilleran Cu-Zn-Pb-(Au-Ag) deposits hosted largely in carbonate sequences (Lindgren, 1935; McKinstry, 1936; Vidal et al., 1984; Bendezú et al., 2003, 2008; Bendezú, 2007). The Cordilleran deposits include Colquijirca and Smelter or Marcapunta Norte (north of the Marcapunta volcanic complex), Marcapunta Oeste (west of Marcapunta), and San Gregorio, one of the largest undeveloped Zn-Pb deposits worldwide (south of Marcapunta, Fig. 1).

Based on $^{40}Ar/^{39}Ar$ dating (Bendezú et al., 2003, 2008), the Cordilleran ores of Smelter and Colquijirca formed during the late hydrothermal history of the Colquijirca district at 10.8 and 10.6 Ma and postdated the episode of high-sulfidation epithermal Au-(Ag) mineralization in the Marcapunta volcanic complex, which formed at ~11.1 to 11.9 Ma in the center of the district, on the southern margin of the Colquijirca and Smelter deposits.

The purpose of this paper is to provide a detailed description of Cordilleran mineralization in the historic Colquijirca district and, in particular, in its northern part, where the Smelter and Colquijirca deposits occur. These deposits form a continuously mineralized corridor that has been extensively explored since 1996, allowing a complete three-dimensional view of the mineral distribution and providing excellent examples of strongly zoned deposits. The paper focuses on mineralogical patterns, carefully documenting zoning and cross-cutting relationships of a well-preserved mineralized system. These mineralogical patterns provide insights into the origin and evolution of the mineralization, in conjunction with fluid inclusion and stable isotope data (Bendezú, 2007).

Terminology

The following terms are employed in the sense of Barton et al. (1963), Barton (1970), Hemley and Hunt (1992), and Einaudi et al. (2003).

"Mineral assemblage:" A group of minerals that occur in direct contact and display no evidence of reaction with one another (Einaudi et al., 2003). Although Hemley and Hunt (1992) applied this term when chemical equilibrium is implied, in this work the term mineral assemblage is strictly descriptive. Minerals that constitute an assemblage are joined with hyphen signs.

"Mineral association:" A group of minerals that occur together but that are not necessarily in contact nor necessarily deposited at the same time (Einaudi et al., 2003). A mineral association implies nonequilibrium conditions (Barton et al., 1963; Hemley and Hunt, 1992). Minerals that constitute an association are separated by commas.

"Stage or single stage of mineralization:" This term is used in the sense of Barton (1970) for a group of phases that represent an interval of deposition during which there is no discernible (major) chemical or physical change.

General Geology

The main feature of the Colquijirca district is the Miocene Marcapunta diatreme-dome complex located in the center of the district. The Marcapunta complex intrudes a thick sequence of sedimentary rocks (Figs. 1, 2), which from the bottom to the top include slates of the Devonian Excelsior Group, red beds of the Permian Mitu Group (Fig. 2), limestones and dolostones of the Late Triassic-Early Jurassic Pucará Group, and continental mainly detrital and carbonate rocks of the Early Cenozoic Pocobamba and Calera Formations (Fig. 1). The main country rocks for Cordilleran mineralization in the Colquijirca district are the carbonate rocks

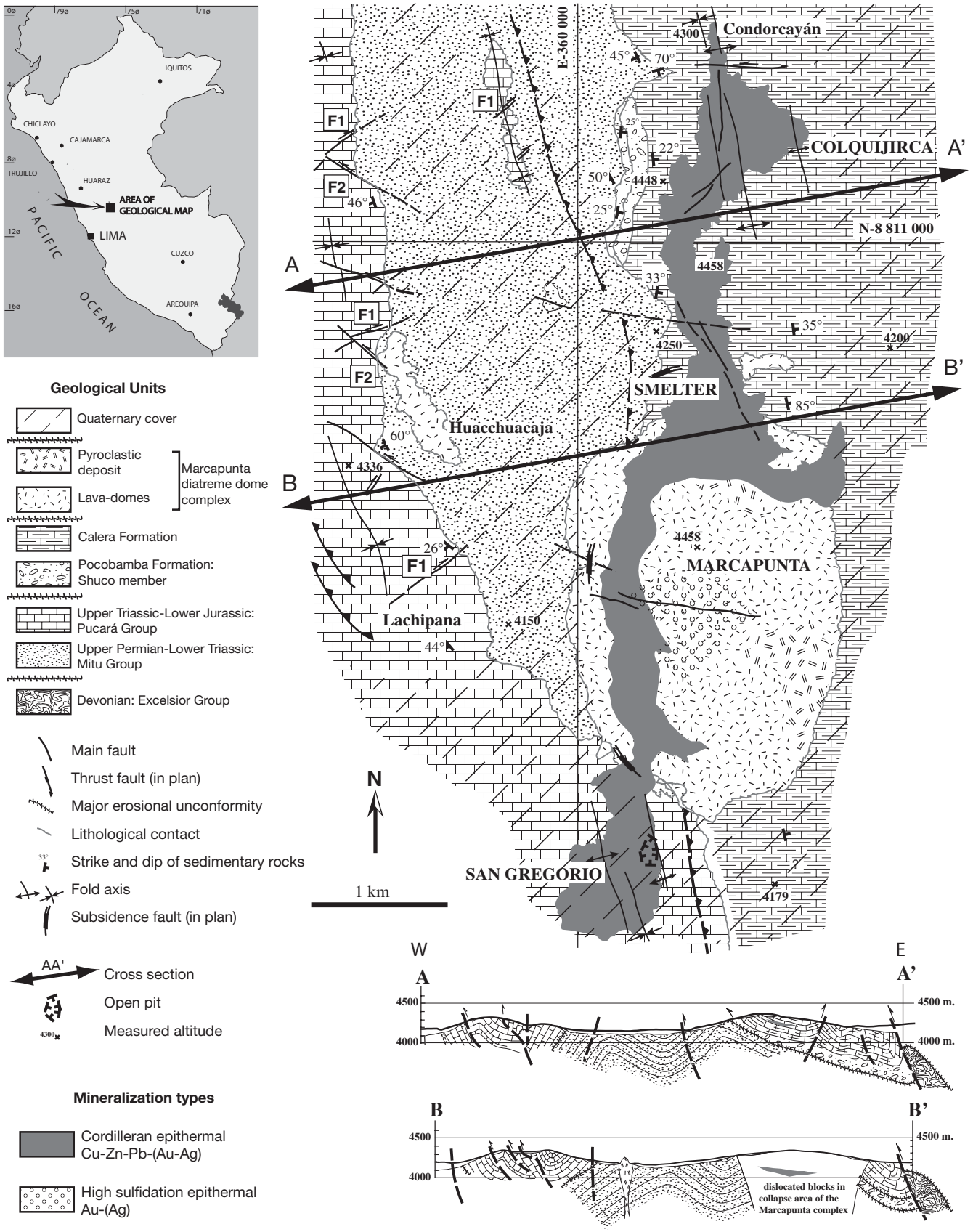

FIG. 1. Location and general geology of the Colquijirca district. Main sources are Jenks (1951), Angeles (1999), Brocal staff, and personal data. Also shown are two geologic cross sections through the northern part of the district.

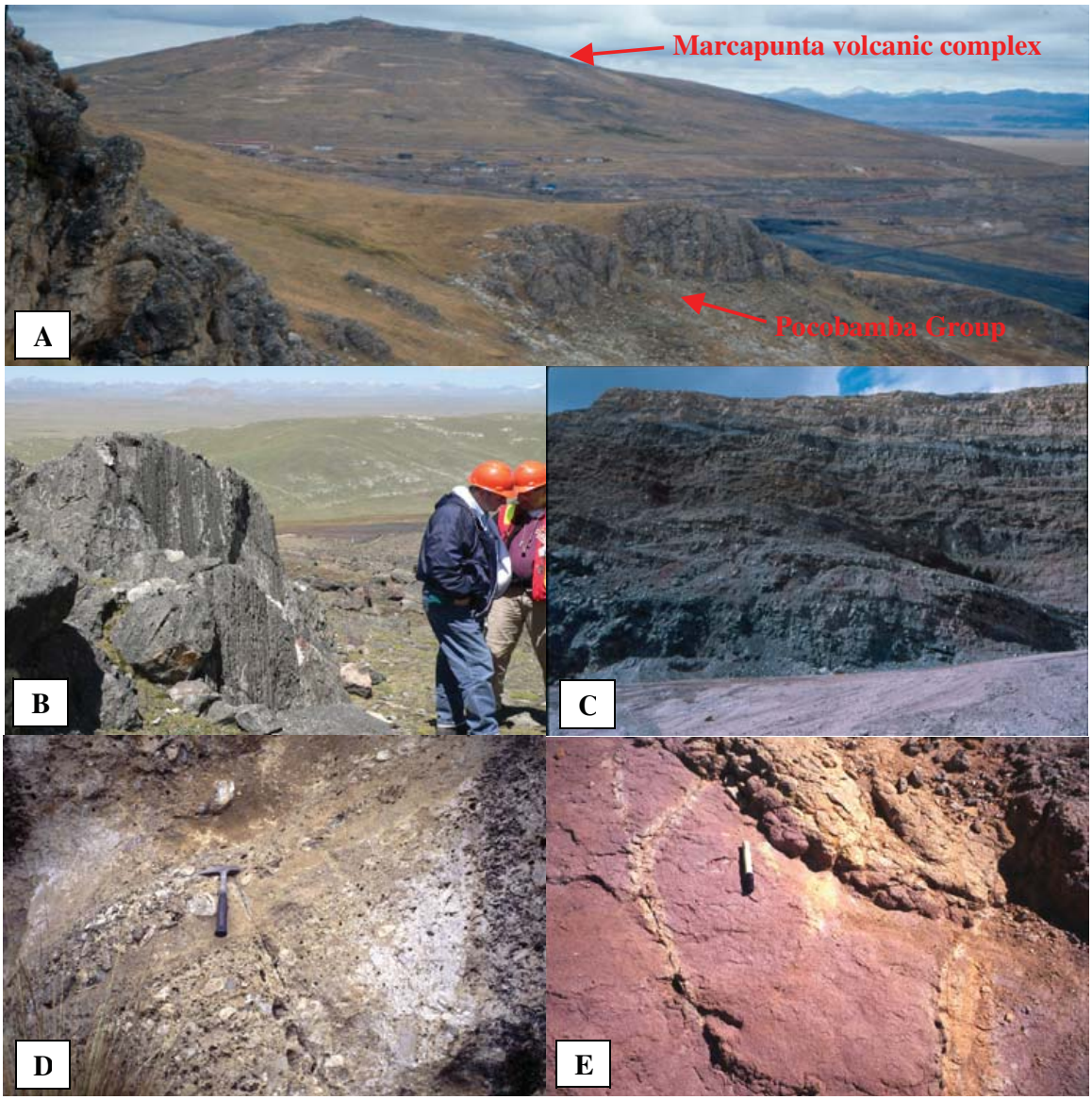

FIG. 2. Photographs of main rock units of the Colquijirca district. A. General view of the northern part of the district looking south. In this sector the Marcapunta volcanic complex intrudes the Pocobamba and Calera Formations that largely host the mineralization at Smelter and Colquijirca. B. Eroded and altered dacitic dome showing well-preserved flow banding. C. Intercalations of limestones, shales, marls, and tuffs of the Eocene Calera Formation. These intercalations are exposed in the former Principal pit at Colquijirca. D. Calcareous conglomerate from the Late Cretaceous Shuco member of the Pocobamba Formation, west of Colquijirca. E. Arkosic sandstone from the Late Permian-Early Triassic Mitu Group red beds, south of Smelter.

from the Pucará Group and the Pocobamba and Calera Formations. The Marcapunta volcanic center is a diatreme-dome complex consisting of multiple porphyritic lava dome intrusions (Figs. 2, 3) of dacitic high K subalkaline composition which pre- and postdate several episodes of phreatomagmatic breccias (D. Noble, pers. commun.,1992; Bendezú et al., 2003; Sarmiento, 2004; Bendezú, 2007).

The Marcapunta diatreme-dome complex has been strongly altered to cores of residual quartz, locally with vuggy texture, with halos of advanced argillic alteration consisting mainly of quartz-alunite- and kaolinite–bearing assemblages. Gold and silver occurring mainly as oxide veinlets and coatings are largely contained in these cores of vuggy quartz. In parts close to the diatreme-dome complex, particularly in the west, the quartz-alunite zones and associated veinlets are cut by centimeter-wide pyrite-(enargite) –rich veinlets and veins generated during the sulfide-rich polymetallic event. $^{40}Ar/^{39}Ar$ dating is in accordance with these crosscutting relationships, indicating that the polymetallic event (~10.8–10.6 Ma) postdated the high-sulfidation Au-(Ag) mineralization (~11.9–11.1 Ma; Bendezú et al., 2008).

The most prominent lineaments in the Colquijirca district are two major regional north-south reverse faults, north-south fold trends, and a strike-slip fault system (F1 and F2 systems,

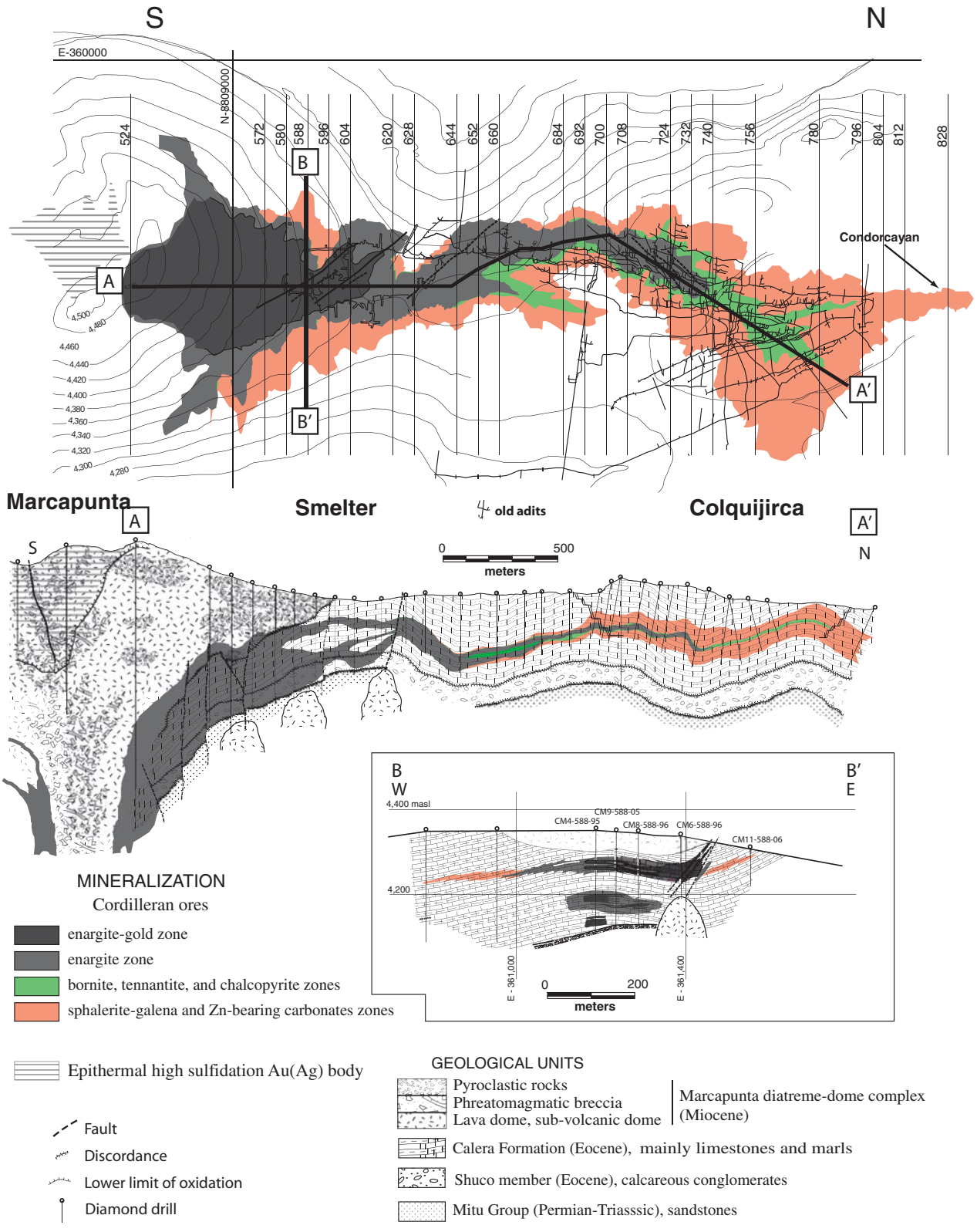

FIG. 3. Mineralization footprint in the northern part of the Colquijirca district, along the Smelter-Colquijirca mineralized corridor. Because of the complex pattern of the mantolike orebodies, only the external limits of ore zones are drawn. A. Plan view of the corridor showing the different ores zones as described in the text. B. North-south composite cross section of the Smelter-Colquijirca mineralized corridor and a selected cross section as indicated in the plant view. Notes: The quartz-pyrite replacement is essentially identical to the enargite zone, and between grid lines 524 and 604 the enargite-gold zone is essentially identical to the enargite zone. Vertical scale is 15 percent larger than horizontal scale.

Fig. 1). According to Angeles (1999) most of these structural elements are related to Neogene compressive events that affected extensive areas of the central and northern Peruvian Andes. Both the folding and F1 and F2 fault systems occurred before hydrothermal mineralization and, as will be shown later, provided important channels for mineralizing solutions, particularly in the northern part of the district.

A detailed review of the geology at regional and district scale is given by Bendezú (2007). In this paper, only the Pocobamba and the Calera Formations, which constitute the main host rock of the Smelter and Colquijirca deposits, are described.

The Pocobamba Formation

The Eocene Pocobamba Formation was first described by McLaughlin (1924). Angeles (1999) divided the Pocobamba sequence into two members. From bottom to top, these are the Cacuán and the Shuco members (Fig. 1).

Cacuán member: The Cacuán member consists of up to 300 m of shales, sandstones, conglomerates, and limestones and can be characterized as a red-bed sequence. Its lower parts are composed mainly of reddish sandstones, siltstones, and mudstones, commonly displaying crossbedding. The conglomerate clasts are <5 cm long, mostly subrounded and cemented by calcareous material, and consist of limestones derived from the Pucará Group (Angeles, 1999), with minor sandstones, siltstones, and locally milky quartz. The upper intervals of the Cacuán member comprise dominantly meter-thick beds of whitish limestones that are lacustrine in origin according to Angeles (1999). At Colquijirca, the Cacuán member is exposed locally at Lachipana hill (Fig. 1; Angeles, 1999).

Shuco member: The Shuco member is 100 to 200 m thick and consists of poorly sorted monomictic, clast-supported breccias and conglomerates (Fig. 2). Near Colquijirca it lies on a variety of pre-Cenozoic rocks, including the Mitu (west of Colquijirca) and Excelsior Groups (at Condorcayán; Fig. 1). Drilling shows that it extends over a large area concealed beneath the Calera Formation in the northern part of the Colquijirca district. Pucará Group pebbles, cobbles, and boulders dominate as clasts. Interclast spaces consist of a mixture of angular to subrounded granule- to cobble-sized material, including sandstone, cemented by calcite. At Colquijirca, immediately west of the operating open pit, the Shuco member exhibits incipient bedding and is dominated by subrounded clasts, most less than 20 cm in diameter (Fig. 2). The Shuco member is considered to be a fanglomerate or piedmont deposit (Jenks, 1951; Angeles, 1999), possibly formed by erosion of mainly Pucará blocks uplifted during the late Mesozoic-early Cenozoic along the north-south longitudinal fault.

Calera Formation

Jenks (1951) described the Calera Formation as composed of about 70 percent argillites, siltstones, and sandstones, and about 30 percent limestones and marls (Fig. 2). Angeles (1999) divided the Calera Formation into three members. The lower member (~60 m thick) is dominated by detrital sediments, including tuffs, sandy siltstones and, to a lesser extent, conglomerate beds decimeter in thickness and consisting of pebbles of black limestone in an argillic matrix. The middle member (~60 m thick) is characterized, by abundant nearly pure carbonate rocks and subordinate meter-thick beds of massive, fine-grained argillites and marls, usually rich in organic matter. The upper member (~150-m thickness) consists of intercalated beds of argillites, siltstones, marly dolostones, marls rich in organic matter, varved carbonaceous dolostones and limestones, and some volcanosedimentary beds, including tuffs.

According to Angeles (1999), the total thickness of the Calera Formation is a minimum of 250 m. Exploration drilling immediately northeast of Marcapunta hill confirms a 500-m-thick sequence. The Calera Formation is thought to be of late Eocene age on the basis of the K-Ar age of ~36 to 37 Ma for biotite from a tuff layer located near the base of the lower member (Noble and McKee, 1999).

Smelter-Colquijirca Mineralization

Mineralization at the Smelter-Colquijirca corridor consists of early quartz-pyrite replacements superimposed by enargite-rich bodies in the parts close to the Marcapunta volcanic complex (mainly at Smelter) and by sphalerite-galena bodies in more distal parts, mainly farther to the north (mainly at Colquijirca). The Smelter deposit is located adjacent to the northern margin of the Marcapunta volcanic complex and occurs between grid lines 524 and 628, whereas the historic Colquijirca deposit is generally considered to occur between grid lines 708 and 804 (Fig. 3). These limits are informally used by Colquijirca geologic staff for resource calculation purposes. Notwithstanding the proximity of Colquijirca to the Smelter deposit, the physical continuity between them was not recognized for a long time (Bendezú, 1997). Stratigraphic correlation of drill cores (see below) demonstrates that Colquijirca is the northern extension of the enargite-rich bodies of the Smelter deposit (Fig. 3).

Host rock

Early-formed extensive quartz-pyrite replacement surrounds the main diatreme conduit and the central volcanic and subvolcanic domes of the Marcapunta complex and affected the entire Pocobamba and Calera Formations, including more than 200 m of the Calera Formation and the Shuco member of the Pocobamba Formation (Smelter deposit, Fig. 3). With increasing distance toward the north, replacement becomes progressively restricted to higher stratigraphic positions within the Pocobamba Formation. This is particularly evident northward from grid line 596 (Fig. 3) where the Shuco member and the lower portion of the Calera Formation are not mineralized (e.g., holes DDH, CM5-596, CM2-604). Farther to the north, the ores at Colquijirca are exclusively hosted in carbonate rocks of the Calera Formation (Fig. 3), in which they specifically replace a 50-to 90-m-thick interval of the Middle member.

At Smelter, mineralization also occurred in the volcanic rocks of the Marcapunta complex. The drill holes located within or near the diatreme conduit (Fig. 3) show lava domes and block and ash deposits up to 10s m thick intensely replaced by quartz and pyrite. An apparently small fraction of the economic minerals occur in the uppermost beds of the Mitu Group red beds, particularly south of grid line 588.

Spatial configuration of the mineralized bodies

The following description is based mainly on evidence from diamond drill holes; where possible, observations in the open pits (Colquijirca) and underground workings (Smelter) have been used.

At a district scale, the volume affected by quartz-pyrite replacement can be roughly depicted as a funnel-shaped body, surrounding at least 75 percent, if not all the main volcanic conduit. In areas close to the Marcapunta volcanic complex, the quartz-pyrite replacement geometry was controlled by the configuration of the contact between the main intrusive conduit and the carbonate host sequence. In more distal sectors, the replacement morphology is basically determined by bedding of the sedimentary host rock and, subordinately, fractures.

The copper orebodies are hosted by the early quartz-pyrite replacements zones along much of the Smelter-Colquijirca corridor. Available drill hole and underground evidence indicates that the copper orebodies are distributed irregularly within the areas of quartz-pyrite replacement and that they commonly display crosscutting geometry controlled by faults and fractures.

At Smelter, in an area extending about 700 to 800 m from the approximate contact between the conduit and the intruded sedimentary rocks, replacement affected the entire section of the Pocobamba and Calera Formations (>200 m thick), including poorly reactive beds of sandstone, argillite, and siltstone. The strong intensity of reaction in this area is also indicated by the fact that intervals up to several ten meters thick of the underlying Mitu Group red beds and overlying volcanic units of the Marcapunta complex were also replaced. Northward from grid line 580 (Fig. 3), replacement is much less intense and preferentially affected monomictic to polymictic breccias of granule to pebble size and highly permeable packstones of the lower part of the Calera Formation. The unreplaced intervals are mainly massive, fine-grained argillites and marls, typically rich in organic matter characteristic of the middle part of the Calera Formation.

As shown in Figure 3, at Smelter, the quartz-pyrite replacement separate into two or, in places, three styles. With increasing distance from the diatreme conduit, the replaced interval becomes narrower and tends to occupy higher stratigraphic positions. Thus, north of grid line 644, replacement is confined to the middle member of the Calera Formation (Fig. 3). The thickness of the quartz-pyrite replacement body decreases considerably north of grid line 700 with less than 20 m in the former Principal pit in the southern part of the Colquijirca deposit (Fig. 3). Northward from grid line 700, Zn-Pb orebodies largely dominate over the quartz-pyrite replacement. Collectively, replacement bodies at Colquijirca form a single 50- to 70-m-thick manto (Figs. 3, 4), which shows continuity over a length of nearly 1.5 km, and up to more than 1,000 m wide, from the Principal pit to the northernmost recognized occurrence at Condorcayán. The manto varies abruptly in strike and dip due to pronounced folding. Thus, it is found either gently dipping, as in the case in the La Pampa flank in the easternmost portion of Colquijirca (Fig. 4), or emplaced semivertically along flanks of anticlines and synclines, as within the tight Mercedes-Chocayoc anticline (Fig. 4).

Individual mantos are typically 2 to 4 m thick, tens of meters wide, and more than 600 m long along strike. Even at the microscopic scale, the bedding control is striking. In places, replacement is observed to mimic bedding to such a degree that sulfide bands are only several tens of micrometers thick. The southernmost high-grade mantos in the Colquijirca deposit are oriented roughly north-south (Fig. 4). Immediately to the north, they are aligned ~N45°E, following a fracture set with this orientation. Farther north the mantos have a south-southeast–north-northwest orientation, along the axis of the Mercedes-Chocayoc anticline and other folds with similar orientation (Fig. 4).

Orebodies in flexures of folds are considerably thicker, and their grades are generally higher than elsewhere; the most spectacular example is found along the entire length of the flexure zone of the Mercedes-Chocayoc anticline, from which most of the bonanza silver grades were exploited underground during the early 20th century (Fig. 4).

In the central portions of the Colquijirca deposit, regardless of the original rock type, virtually all beds of the middle part of the Calera Formation were completely replaced to leave no significant relicts. The outermost individual mantos are in many places separated from others by relatively unreactive units such as massive argillites or argillaceous tuffs; locally, intervals of fine-grained, massive dolostones intercalated with the mineralized mantos occur in these external portions. On the basis of stratigraphic markers the stratigraphic position of the mineralized interval is ~50 m higher at the northernmost observed occurrence at Condorcayán in contrast with the southern part of the Colquijirca deposit, a distance of nearly 1,500 m (Bendezú, 2007).

Mineral Deposition: Stages and Zoning

The spatial configuration of orebodies, crosscutting relationships at different scales, and the study of more than 150 thin sections from the northern block of the district (Tables A5, A6) have allowed discrimination of three mineral stages (Fig. 5). The stages are (1) an early quartz-pyrite stage that produced the large, basically barren, quartz-pyrite replacement bodies from Smelter to Colquijirca; (2) the main ore stage of arsenical Cu-(Au) minerals, located around the volcanic complex at Smelter, and rich Zn-Pb-(Ag) ores in the distal portion of Colquijirca; and (3) a late ore stage which generated economically less important gold-free copper minerals at Smelter.

Early Quartz-Pyrite Stage

In any portion of the Smelter deposit and also in the southern part of Colquijirca, an early preore stage composed essentially of quartz and pyrite is present. This stage, although economically unimportant, is by far the most important in terms of volume. An estimated 800 to 1,000 million metric tons (Mt) containing an average of 40 to 50 vol percent pyrite is present in the Smelter-Colquijirca mineralized corridor, and a similar volume probably exists in the recently defined Marcapunta Oeste resource.

In the Calera Formation, the quartz-pyrite stage forms mainly simple replacement of limestones and/or dolostones, marls, calcareous argillites, and conglomerates, the original fabric of the host rock being commonly preserved (Fig. 6B).

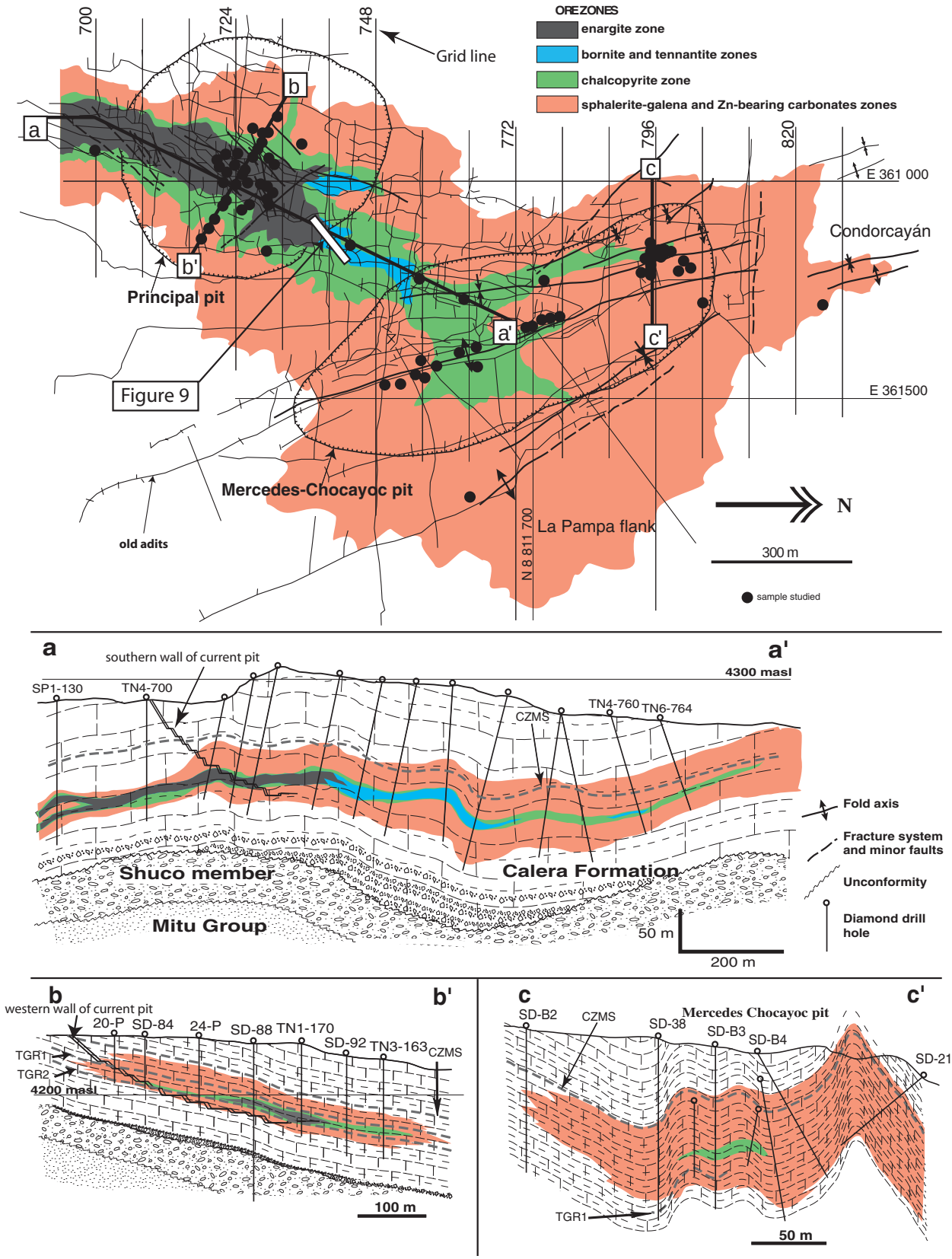

FIG. 4. Plan view of the northern sector of the Colquijirca district (Colquijirca deposit), showing the main ore zones projected to the surface. Selected samples studied in this work are also shown. Old silver workings largely followed the main axis of the deposit. Three sections, with locations in the plan map, have various scales. Stratigraphic markers CZMS and TGR1 and TGR2 are shown.

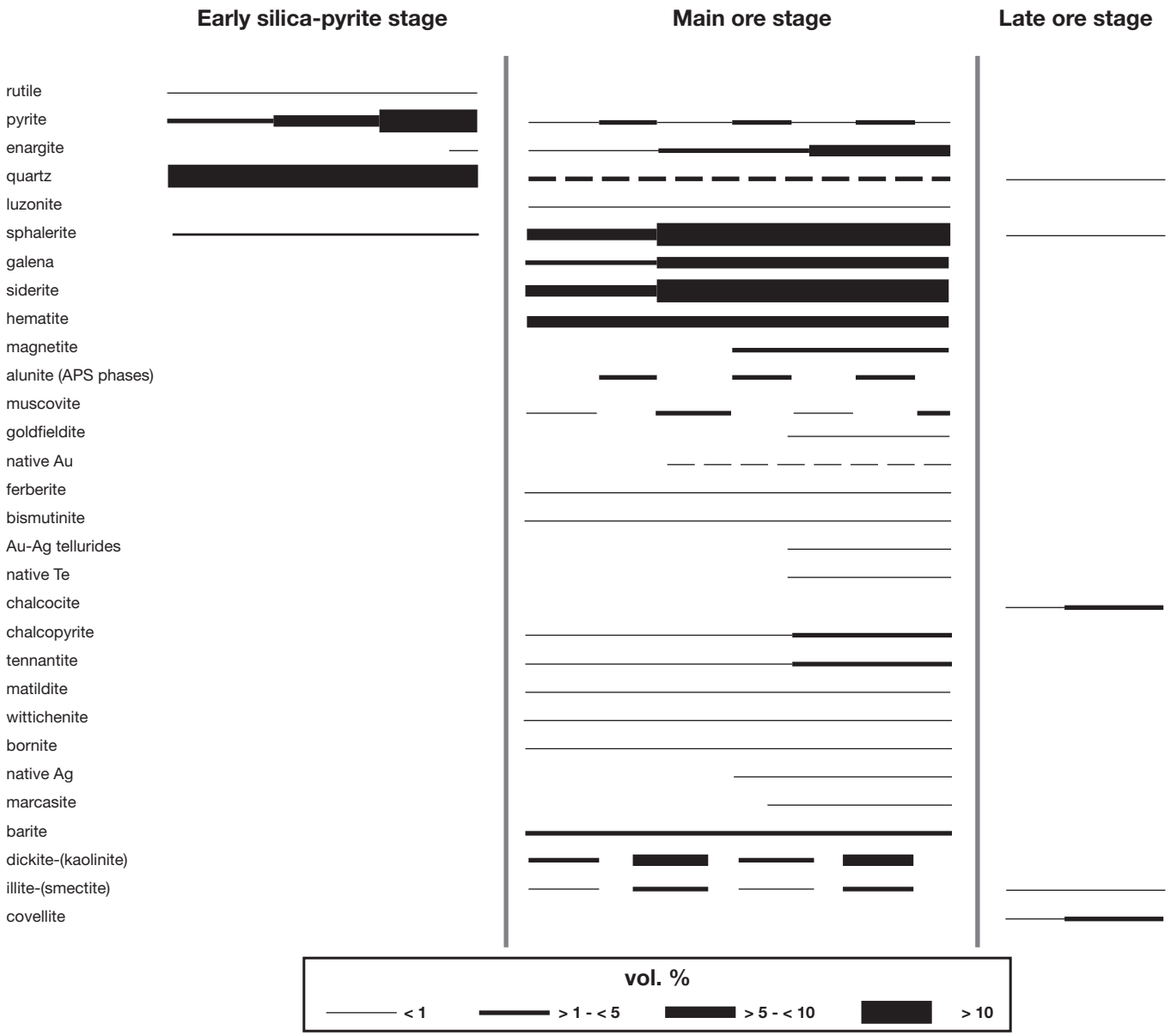

FIG. 5. Mineral paragenesis in the Smelter-Colquijirca corridor.

Finely laminated bands as thin as a few tens of microns composed of alternating pyrite- and quartz-rich bands also occur, particularly toward the top of the mineralized sequence. These banded intervals correspond to varved carbonaceous dolostones and limestones, typical of the upper member of the lacustrine Calera Formation. It is relatively common to observe biogenic textures completely replaced by quartz-pyrite.

Strongly silicified and pyritized conglomeratic beds characterize the sequence below the Calera Formation; they consist of alternating clast- and matrix-supported breccias, both with well-rounded monomictic clasts of various sizes. This breccia may represent replaced sedimentary breccias and conglomerates from the Shuco member. Relatively rare hydraulic breccias, more common crackle breccias, as well as breccias with monomictic to heterolithic clasts (partly showing dissolved margins and internal sedimentary structures) are present in the Calera Formation (Fig. 6A). The clasts, up to 20 cm in diameter, of the sulfide-poor breccias are derived from carbonate and/or detrital rocks texturally identical to the hanging-wall rock. Matrix accounts for 40 to 60 percent of the breccia.

Replacement mineralogy

Quartz accounts for at least 60 vol percent of the quartz-pyrite replacement bodies. It occurs mainly as subhedral to subordinate euhedral grains ranging in size generally between 30 μm to 2 mm. Other siliceous rocks are cryptocrystalline and, in order of decreasing abundance, consist of chert, jasperoid, and rare, an extremely fine grained silica phase, possibly opal. Chert appears dark in color; commonly almost black (Fig. 6E). Under the microscope, dark chert, which accounts for about 10 to 20 percent of the total mass of siliceous rock, is composed of quartz crystals 5 to 20 μm in diameter,

TABLE 1. Main Mineral Assemblages from the Early Quartz-Pyrite Stage, Main Ore Stage, and Late Ore Stage (relative abundance of minerals are represented in Figure 5)

	Early quartz-pyrite stage
	Pyrite-quartz-chlorite-muscovite-rutile-scheelite
	Pyrite-quartz-chlorite-muscovite
	Main ore stage
Enargite-gold and enargite zones	Enargite-luzonite-pyrite-bismuthinite-alunite-zunyite-quartz
	Enargite-luzonite-pyrite-kaolinite-dickite
	Enargite-luzonite-ferberite-pyrite-illite-smectite
	Enargite-luzonite-pyrite-muscovite
	Enargite-luzonite-electrum
	Pyrite-alunite-quartz
	Colusite-stannoidite-vinciennite?-pyrite-zunyite-alunite-quartz
	Tennantite-goldfieldite-gold and silver tellurides-native tellurium-electrum
Bornite zone	Bornite-pyrite-sphalerite-mawsonite?-dickite-kaolinite-quartz-barite-APS minerals?
Tennantite zone	Tennantite-pyrite-native silver-barite-quartz
	Tennantite-pyrite-chalcopyrite-stromeyerite-emplectite-native silver-dickite-kaolinite-barite-quartz
Chalcopyrite zone	Chalcopyrite-tennantite-pyrite-galena-matildite-wittichenite-quartz-dickite-kaolinite-barite-siderite
	Chalcopyrite-pyrite-sphalerite-galena-quartz-dickite-kaolinite-barite
Sphalerite-galena zone	Sphalerite-galena-pyrite-quartz-alunite-barite
	Sphalerite-galena-pyrite-kaolinite-dickite-barite
	Sphalerite-galena-pyrite-siderite-kaolinite
	Sphalerite-galena-pyrite-siderite-hematite-magnetite
Zn-bearing carbonates zone	Zn-bearing siderite-rhodochrosite
Barren outer zone	Calcite-dolomite
	Late ore stage
	Chalcocite-digenite-covellite

along with variable amounts of unidentified extremely fine grained material. Jasperoid can be locally dominant (Fig. 6C). From microscopic observations, hematite inclusions give the reddish color. The fine-grained silica phase occurs with banded colloform textures and rarely as alternating colorless and white bands (Fig. 6D).

Northward from grid line 740, at Colquijirca, numerous beds (<2 m thickness) of chert characterize the early quartz-pyrite stage and occur persistently along the most distal parts of the Colquijirca deposit as well as at Condorcayán. The beds are most commonly composed of dark to black cryptocrystalline quartz and finely crystallized quartz that, in general, make up no more than 30 vol percent of the rock. Under the microscope, the beds contain <5 vol percent of pyrite inclusions, <100 μm in size. The pyrite is generally slightly corroded.

Pyrite from the early quartz-pyrite stage represents more than 90 vol percent of the total sulfides of the entire Smelter-Colquijirca corridor. Pyrite is most commonly octahedral, ranging in size from 20 μm to 1 mm but mainly between 20 μm and 0.4 mm (Fig. 6G). Grains are corroded, but the octahedral shape is still recognizable. Other less common forms are cubes and, more rarely, pentagonal dodecahedra. SEM imagery reveals that pyrite is commonly finely zoned in arsenic and, to a lesser degree, copper. Microprobe analyses indicate As up to 1.2 wt percent (typically 0.2–0.6 wt %; Table A1), and copper typically <0.2 wt percent, although locally >1 wt percent. This early pyrite is termed pyrite I. The early quartz-pyrite stage also includes minor to trace quantities of extremely fine grained rutile, zircon, and scheelite disseminated in the quartz-pyrite matrix (Fig. 6H). More rarely, muscovite and locally also chlorite were identified through Raman spectroscopy and occur as radial aggregates and isolated acicular grains encapsulated in quartz. These phases are too fine (usually <10 μm) and in concentrations too low to be studied by other conventional techniques. The presence of muscovite is consistent with the mineralogical composition of the external haloes to the quartz-pyrite replacements at the deposit scale, which display, in thin section, remnant muscovite-quartz ± pyrite assemblages. These remnant haloes are only observed around quartz-pyrite replacements developed in the volcanic host rocks in the upper parts of the mineralized sequence, below the northern flank of Marcapunta. Chalcopyrite, sphalerite, marcasite, and pyrrhotite occur as minute inclusions in pyrite.

The early quartz-pyrite stage displays a gradual increase in pyrite with growth, recognized from crosscutting relationships in vein-dominated zones where pyrite-rich veinlets cut pyrite-poor ones (Fig. 6A, F). Pyrite abundance as well as grain size increase from trace to over 60 vol percent in the latest veinlet generations. The increasing abundance of pyrite with time occurs in the breccias, where several generations of matrix and veins are observed. The late vein generations consist mainly of pyrite, whereas the matrix and clasts replaced in the early stages show only minor pyrite disseminations (Fig. 6F).

Main Ore Stage

There is no evidence for a time gap between termination of the early quartz-pyrite stage and the main ore stage. Some samples display late quartz-pyrite veinlets accompanied by minor to trace amounts of enargite, suggesting that transition between the early quartz-pyrite stage and the main ore stage was gradational.

Abundant crosscutting relationships indicate that the main ore-stage fluids extensively overprinted the early stage. The quartz-pyrite in internal parts was mainly overprinted by minerals of the copper-bearing ore zones. Beyond the quartz-pyrite front the overprinting was mainly by minerals of the zinc-lead–bearing zones. From internal to external portions, the main ore-stage zones consist of (1) enargite ± (luzonite, pyrite, colusite, tennantite, goldfieldite, ferberite, gold-silver tellurides, bismuthinite, gold, alunite, zunyite, kaolinite, dickite, smectite, illite, muscovite, quartz); this zone is termed the "enargite-gold zone;" (2) enargite ± (pyrite, quartz, bismuthinite, alunite, dickite, kaolinite, smectite, illite, muscovite) is

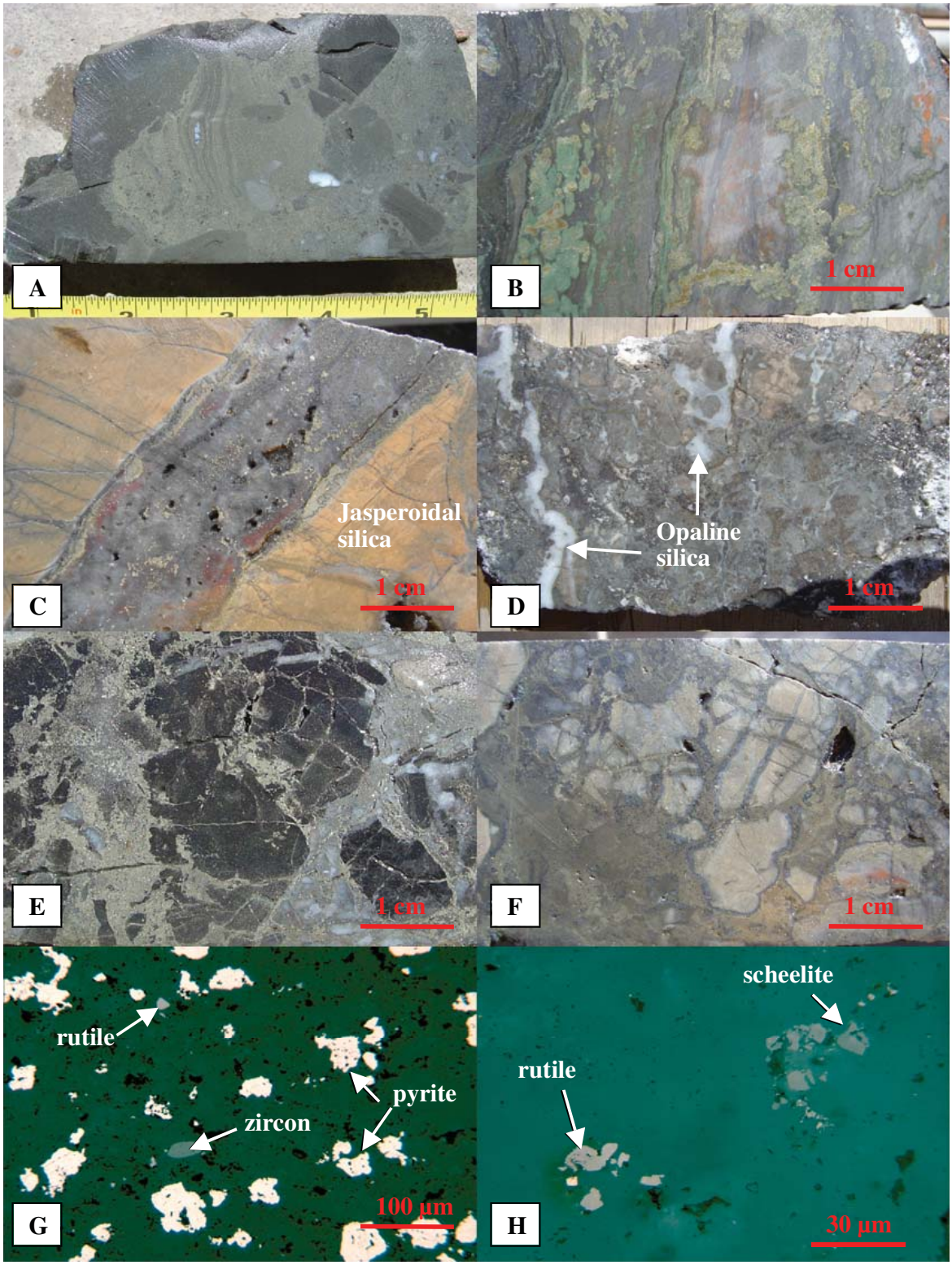

FIG. 6. Photographs of typical occurrences of the early quartz-pyrite stage. A. Nearly massive pyrite replacement of a conglomeratic bed. B. Quartz-pyrite replacement of laminated limestones of the Calera middle member. Possible biogenic textures now replaced by pyrite. C. Quartz-pyrite veinlets cutting silicified limestone. The wall rock of the thick veinlet is jasperoid. D. Pyrite-poor silicified limestone. Part of the fine-grained silica phase, similar to opal. E. Typical dark chert produced by silicification of argillite. F. Typical sequence of quartz-pyrite precipitation ranging from nearly pyrite-free replacement to younger pyrite-rich veinlets and replacements. G. Polished section photomicrograph showing typical fine-grained pyrite disseminations in a quartz matrix. Rutile and zircon are accessory phases. H. Polished section photomicrograph showing rutile and scheelite grains in a quartz matrix.

referred to as the "enargite zone;" (3) bornite ± (pyrite, quartz, alunite, dickite, kaolinite, barite), termed the "bornite zone;" (4) tennantite, barite ± (dickite, kaolinite, chalcopyrite, Bi and/or Ag-bearing minerals), the "tennantite zone;" (5) chalcopyrite, sphalerite, galena ± (pyrite, quartz, dickite, kaolinite, barite), the "chalcopyrite zone;" (6) sphalerite, galena, pyrite ± (hematite, kaolinite, siderite, magnetite, marcasite), the "sphalerite-galena zone;" and the (7) "Zn-bearing carbonate zone." A "barren outer zone" occurs commonly beyond the Zn-bearing carbonate zone.

Enargite-gold zone

The enargite-gold zone typically contains 1 to 2 percent Cu and 0.2 to 1.0 g/t Au. Enargite comprises up to about 90 vol percent of the total sulfide content. Enargite is commonly intergrown with its polytype luzonite (about 5 vol %) and with variable amounts of mainly pyrite, colusite, tennantite, goldfieldite, ferberite, gold-silver tellurides, bismuthinite, gold, quartz, alunite, zunyite, kaolinite, dickite, smectite, illite, and muscovite. The enargite-gold zone is present 800 m below the surface at Marcapunta in narrow subvertical veins and veinlets that are interpreted to represent the roots of the epithermal polymetallic system. Horizontally, the enargite-gold zone extends northward to approximately grid line 620 (Fig. 3).

Enargite ranges in size from a few millimeters up to 5 cm and in most cases is coarse grained, commonly anhedral to locally subhedral; intergrain cavities between late generation pyrite-rich clusters of the quartz-pyrite stage are filled, accounting for up to 60 vol percent of the enargite (Fig. 7A). Elongate prismatic crystals are common and found in druse-like cavities in both veins and mantos. Intervals of massive enargite (up to >2 m thick) composed of anhedral grains are also present, with infrared evidence that enargite commonly underwent dissolution and recrystallization (Fig. 8B).

Luzonite is most typically intergrown with anhedral-subhedral grains of enargite (Fig. 7H). In polished section, luzonite is distinctly more pinkish than enargite and commonly displays fine polysynthetic twinning under crossed nicols. Irregular masses of luzonite without evident twinning almost completely replace enargite. Luzonite replaces enargite mainly along twinning and more rarely is replaced by enargite, mainly along grain contacts.

Although much less abundant (5–10 vol %) than in the early quartz-pyrite stage, pyrite also precipitated during formation of the enargite-gold zone and is the next most abundant mineral after enargite. The main style of this pyrite, here termed pyrite II, fills veinlets up to a few centimeters thick, which partly grade into open spaces following bedding. These open spaces and veinlets commonly lack enargite and contain, in order of decreasing abundance, alunite, quartz, and zunyite. Pyrite II occurs also as repetitive thin bands intergrown with enargite (Fig. 7C), is largely subhedral to euhedral and coarse grained (up to 1 cm in size), and commonly forms pyritohedra, whereas octahedral and cubic forms, typical of pyrite I, are rare. In polished section, pyrite II displays remarkable zoning due mainly to alternation of dense and porous bands, which contain voids up to several hundreds of microns long thought to be remnants of fluid inclusions and/or of anhydrite. A second zoning type is due to compositional variations (see below), which are commonly expressed by differential surface oxidation on exposure of the sulfide to air.

Much of the pyrite II occurs in spatial association with enargite-rich zones. Less commonly, pyrite II occurs directly overprinting early quartz-pyrite bodies that are essentially enargite free. In such cases, only quartz accompanies pyrite II, with 2 to 5 vol percent of pyrite II occurring as tiny subhedral grains replacing enargite.

Gold in the enargite-gold zone is recognized in two paragenetic positions. Early deposition occurred as irregular inclusions of electrum, elongate and <10 μm long, (>90 wt % Au and <10 wt % Ag, see below), within enargite. Electrum grains are mainly located either along the cleavage or between grains of enargite, suggesting that the gold precipitated together with enargite or postdated it. In a few examples, the grains partially fill minute cavities in enargite without any apparent crystallographic control; again the gold could have precipitated with or later than enargite. The tiny gold inclusions were probably deposited relatively late in the main ore stage because most of the electrum occurs with the latest enargite generations.

A second occurrence of gold is associated with blebs, up to 50 μm in diameter, of Te-bearing phases, including locally abundant goldfieldite and tennantite (Fig. 7E); the blebs replace late generations of enargite along grain boundaries. Gold occurs chiefly as tellurides, with minor amounts of extremely fine grained electrum (<5 μm in size) as inclusions in goldfieldite, including kostovite (Fig. 7F) and nagyagite. Goldfieldite is zoned and alternates with bands of tennantite, with overgrowths of Te-bearing phases and tennantite on enargite grains (Fig. 7E).

Silver tellurides also occur in blebs similar to those with gold tellurides. Microprobe analyses (Table A2) prove the presence of stutzite and combined energy-dispersive system (EDS) tests and polished section properties suggest the presence of hessite (Fig. 7F). These and other unidentified silver tellurides occur intricately intergrown with the gold tellurides, goldfieldite, and native tellurium (Fig. 7F); these silver minerals do not contribute substantially to the silver values found in most argentiferous intervals.

Two inclusions of native iridium in enargite, both only a few microns in size were recognized through EDS tests and optical properties in polished section. Like the tiny electrum inclusions in enargite, iridium deposition is assigned to the main ore stage.

Colusite is a common minor mineral in the enargite-gold zone. Colusite mainly occurs as strongly zoned euhedral grains up to 1 mm wide of pyritohedral to cube shapes. The colusite shows sector zoning and stronger reflection pleochroism than that described by Ramdohr (1980) and typically replaces enargite and especially pyrite II. Only locally does enargite replace colusite along fractures, cleavage, and growth planes. Some pyrite II shows no reaction effects against colusite, suggesting that, in places, they may constitute an equilibrium assemblage. Moreover, much of the colusite is observed to be in reaction-free contact with alunite, zunyite, and quartz (Fig. 7D).

Stannoidite is a minor to trace tin mineral, commonly but not necessarily associated with colusite, and occurs as irregular blebs on the edges of quartz, enargite, or alunite clusters.

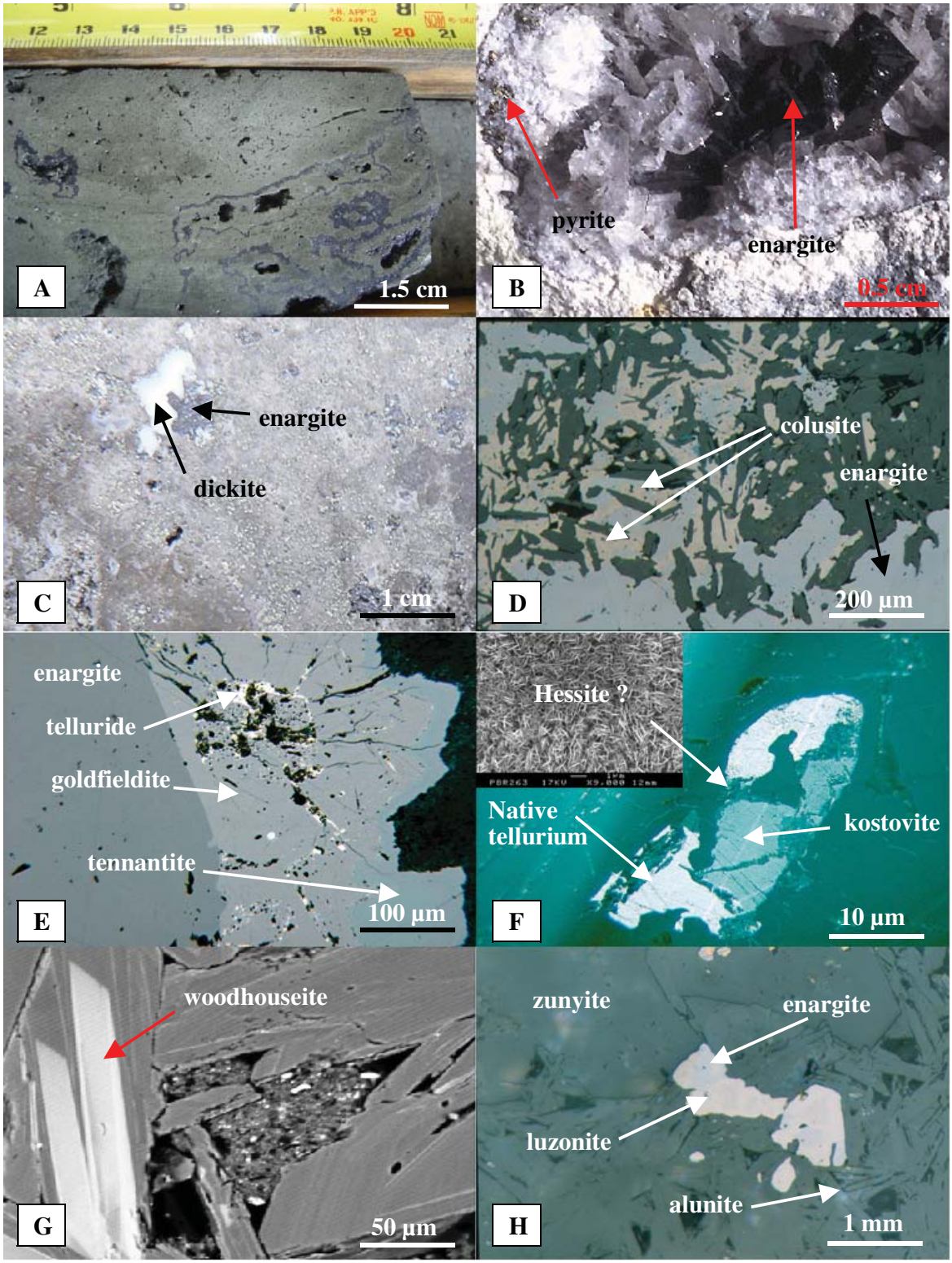

FIG. 7. Representative images of mineral associations and assemblages from the enargite-gold zone. A. Massive sulfide sample consisting of pyrite from the early quartz-pyrite stage enargite, and pyrite II from the main ore stage. Note repetitive sequences of crystallization between bands of pyrite II and enargite. B. Enargite intergrown with alunite and pyrite in a small geodelike cavity. C. Enargite in contact with dickite showing no reaction effects. D. Alunite postdating enargite. Colusite appears to have formed as a product of the reaction between enargite and alunite. E. Tennantite-goldfieldite and associated tellurides growing on younger enargite. F. Oil immersion image of native tellurium partially replaced by kostovite and hessite? G. BSE image of APS grains made up of cores of the woodhouseite series and rims of alunite. H. Polished section image showing an alunite-zunyite assemblage accompanied by luzonite filling intergrain spaces.

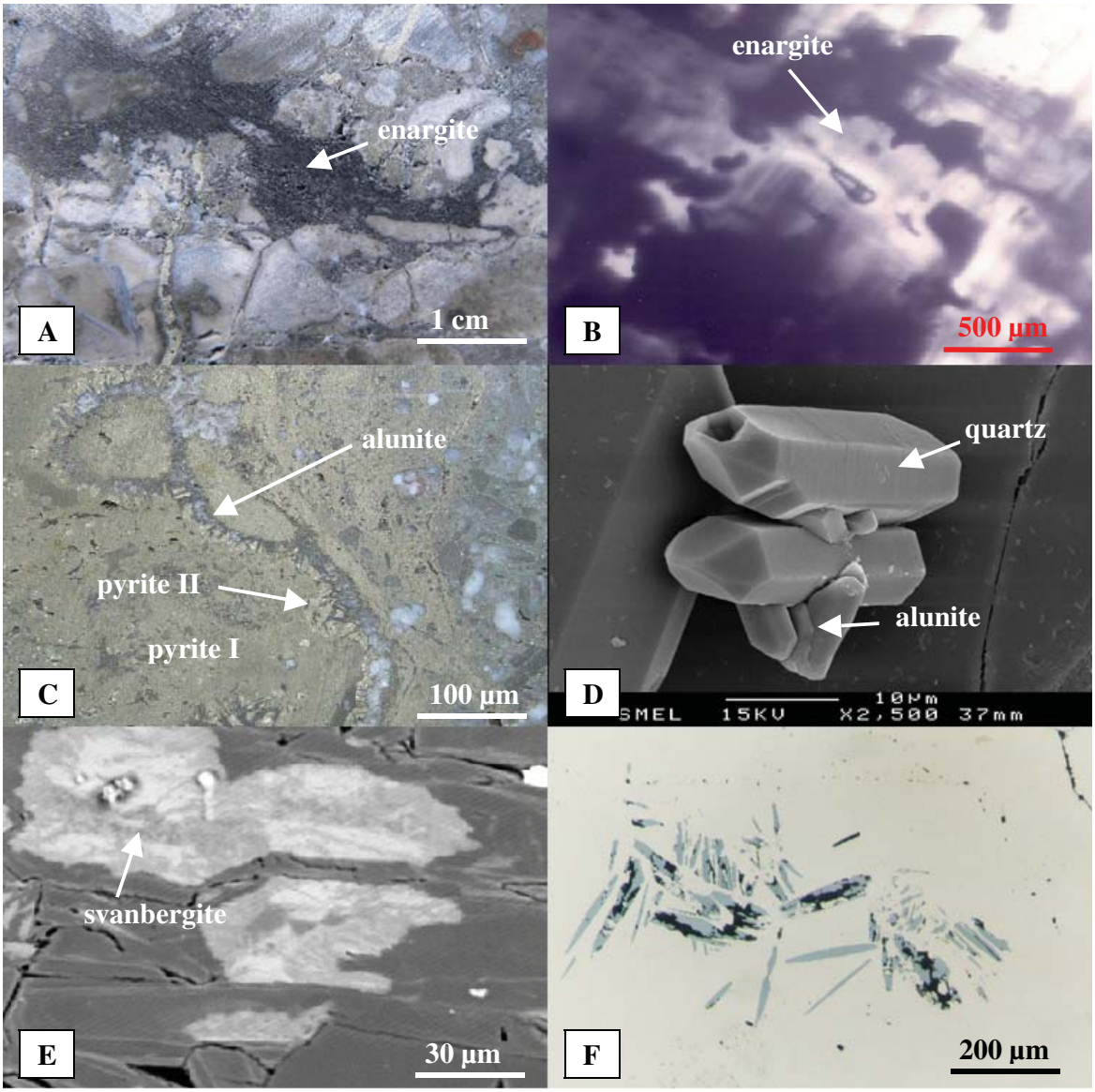

FIG. 8. Representative images of mineral associations and assemblages from the enargite zone. A. Enargite replacing a conglomeratic rock. Enargite is macroscopically devoid of nonopaque gangue minerals other than quartz, however this sample contains trace amounts of illite-smectite as revealed by Raman spectroscopy. B. Enargite observed through infrared imagery. Note corrosion of enargite controlled by growth and cleavage planes. In this sample the enargite is cut by quartz-alunite veinlets. Note also a primary fluid inclusion. C. Undulant bands of barren quartz-alunite-pyrite II replacing massive pyrite from the early quartz-pyrite stage. D. Secondary electron image of a barren quartz-alunite veinlet showing detail of reversed crystallization between alunite and quartz (quartz growing on alunite and alunite on quartz). E. BSE image showing grains of APS group minerals consisting of corroded cores of the svanbergite series and rims of alunite. F. Specular hematite partly replaced by main ore-stage pyrite.

In general, where stannoidite and colusite are in contact, the former replaces the latter. A second extremely fine grained accessory phase is observed intergrown with colusite. Optically it resembles vinciennite, but a definitive identification is lacking.

Ferberite, though usually in trace quantities, is common in the enargite-gold zone. Euhedral prismatic grains, some of which are twinned and up to >100 μm in size, were observed in numerous enargite-rich samples. Ferberite mainly occurs paragenetically earlier than enargite and main ore-stage quartz (quartz II, see below).

Another common accessory mineral of the enargite-gold zone is bismuthinite, which may be locally abundant (up to 1 vol %). It occurs as minute inclusions, exclusively in enargite. In similar form, unidentified Bi and Ag minerals, shown by EDS tests, may have been introduced coevally. Economic argentiferous intervals may in part be explained by these Ag-bearing phases. The observations indicate that all these extremely fine grained phases tend to be more abundant in late enargite generations.

The main alteration minerals include, in order of abundance, alunite, quartz, and zunyite that together constitute

between 30 and 40 vol percent of the main ore stage. Approximately 40 percent of the enargite in the enargite-gold zone is found in direct contact with alunite ± (zunyite). Commonly, alunite accompanied by quartz and subordinate pyrite forms veinlets that cut and/or replace enargite. A reversed paragenetic sequence is also common, mainly as enargite filling intergranular spaces within alunite. Most of the enargite in contact with alunite that precipitated paragenetically late displays the effects of strong corrosion and recrystallization, up to complete loss of the original grain morphology, based on infrared imagery (Fig. 8B). In other cases colusite rims (without reaction) clusters of alunite and replaces the enargite matrix (Fig. 7D), whereas euhedral grains of alunite in open spaces less commonly occur intergrown with enargite (Fig. 7B) and more rarely also with sphalerite.

As mentioned above, alunite, quartz, and zunyite are also commonly found in pyrite II veinlets devoid of enargite, where alunite occurs largely as platy euhedral grains intimately intergrown with quartz and zunyite (Fig. 7H). The best-developed and largest grains, up to 5 mm across, are pinkish and translucent and occur in small geodes and fractures. Reversals in crystallization sequences without evidence of reaction between pyrite II-alunite and pyrite II-quartz pairs are common (Fig. 8D). Euhedral pyrite II grains are encapsulated in alunite and vice versa, which suggests that alunite, pyrite II, and quartz were precipitated essentially simultaneously and in chemical equilibrium.

Alunite displays highly variable birefringence with a relatively well defined pattern depending on the distance to the Marcapunta magmatic center. The birefringence attains second-order blue in the innermost parts, with a tendency to lower first-order gray to yellow in the rest of the zone. Observation with the SEM shows that the alunite usually contains two discernible phases of aluminum phosphate sulfate (APS) group minerals (Fig. 7G). Cores identified with microprobe analysis are dominated by the woodhouseite series, whereas rims are essentially pure alunite (see below). The cores generally display well-developed oscillatory zoning with dense bands, which become progressively less abundant toward the grain borders.

Zunyite is widespread throughout the entire enargite-gold zone and consists of euhedral tetragonal pyramids (Fig. 7H), in places with a truncated octahedral form, up to 2 mm wide and translucent. Zunyite without alunite is uncommon. The mutual relationships of the pyrite II-zunyite pair are similar to those of pyrite II-alunite. For example, euhedral pyrite grains are encapsulated within zunyite but the reverse, although rarer, has also been noted.

Quartz is slightly less abundant than alunite-(zunyite). In common with the distinction made between early-stage pyrite I and main ore- stage pyrite II, quartz deposited during the main ore stage is called quartz II, which is typically euhedral and highly variable in grain size. Tiny grains occur in intricate intergrowths with alunite and zunyite as part of pyrite II veinlets; larger quartz grains are intergrown with enargite but lack the alunite-zunyite pair. Minor amounts of clay minerals are observed locally accompanying this quartz. Quartz with enargite is commonly corroded where in contact with later alunite.

Minor to trace amounts of dickite, kaolinite and, in places, smectite and illite are present throughout the enargite-gold zone, particularly in portions devoid of alunite-bearing assemblages. These clays typically fill intergranular spaces in enargite, pyrite II, and quartz II. In general, where kaolinite and dickite are in contact with enargite, no reaction is observed (Fig. 7C). Furthermore, kaolinite, dickite, and also illite occur as inclusions in enargite, with no reaction effects.

Numerous meter-wide intervals consisting of enargite-rich ores contain only trace amounts of illite-smectite and muscovite-filling enargite and/or pyrite intergranular spaces, or as inclusions in enargite. Again, no reaction is observed between illite-smectite, and muscovite with enargite. The common occurrence of clays and muscovite in alunite-free enargite bodies is consistent with the results of a systematic study of the clays of the Smelter deposit (J. Diaz, pers. commun., 1998). Minor amounts of specular hematite are partially to nearly completely replaced by pyrite II (Fig. 8F).

Composition of minerals in the enargite-gold zone: Enargite and luzonite are nearly stoichiometric (Table A1). Antimony contents are below 1.5 wt percent in the enargite and slightly higher (up to 2.0 wt %) in the luzonite. Tin contents are higher (0.3–1.5 wt % in enargite and up to 3.0 wt % in luzonite) than zinc and bismuth (<0.3 wt %), and silver contents are lower (0.1–0.3 wt %, locally up to 0.6 wt %).

Main ore-stage pyrite II contains significant arsenic (up to 0.6 wt %) and copper (from 0.5–1.5 wt % and up to 4 wt %). Einaudi (1968) found similarly high copper at Cerro de Pasco. Silver ranges from below detection limit to 0.4 wt percent. Pyrite II in inclusions in enargite is in general rich in copper (up to 3.2 wt %).

Goldfieldite, the Te-rich end member of the tennantite series, contains up to 23.6 wt percent tellurium (Table A2). Antimony substitution for arsenic is important (generally between 1.5–5.2 wt %); well-developed zoning in some grains is likely due to such Sb variations. Bismuth concentrations are between 0.2 and 2.0 wt percent. Other minor elements detected in significant concentrations are silver and vanadium, up to 0.8 and 0.3 wt percent, respectively. Five samples indicate that tennantite associated with goldfieldite and gold-silver tellurides contains up to 7 wt percent Fe. In these samples, substitution of arsenic for antimony is minor (Sb content generally <1.5 wt %). Silver contents are in general <0.1 wt percent (Table A2).

Sixteen grains of electrum, all part of the first gold deposition period of the main ore stage, were sufficiently large for microprobe analysis. Electrum has a relatively homogeneous composition, ranging from 84 to 94 wt percent Au with the remaining fraction consisting of silver (Table A3). In a few grains, there is up to 4 wt percent Cu.

The native tellurium analyzed is nearly pure. Only minor concentrations of Cu and Au were detected in the five analyzed points (<0.4 and 0.3 wt %, respectively, Table A3). Analyses of some of the other accessory minerals from the main ore stage of the enargite-gold zone, including stannoidite, kostovite, and stutzite are given in Table A2.

Colusite compositions are close to stoichiometric (Table A1). Elemental substitution in the R site (Sn, As, Sb) suggests a relationship between the strong zoning and compositional variations. For example, tin ranges from 4.9 to 9.2 wt percent

in a single grain, coincident with a decrease in As + Sb from 10.4 to 5 wt percent. The few analyzed grains of stannoidite are essentially stoichiometric (Table A2). A few analyses of sphalerite accompanying alunite and enargite gave FeS contents between 0.08 and 0.21 wt percent.

Over 50 analyses from six widely spaced alunite samples from the enargite-gold zone were analyzed using the electron microprobe (Table 2). High-energy bands in SEM images, observed in the cores of grains, are generally rich in P_2O_5 (0.12–0.20 wt %), with the A site largely occupied, to varying degrees, by Sr, Ca, and Pb (woodhouseite series). These woodhouseite series bands are the most enriched in fluorine (up to 2.1 wt %; Table 2). Toward the rim, the high-energy bands are less abundant, giving rise to homogeneous and wide low-energy bands that are rich in K (alunite end member), with Na/K <0.1 and virtually free of Sr, Ca, and Pb. Where the cores of the grains consist of a single zone, usually corroded, it is even more enriched in P_2O_5 (up to 0.54 wt %) but Pb free and, more rarely, Ca free. In such examples, the core may reach the svanbergite end-member composition (Fig. 8E). A particular feature of this second type of core is its high cerium content. The rim in this second case is also alunite with similar Na/K values (<0.1). This type of alunite containing a core of svanbergite tends to be more abundant in the outer portions of the enargite-gold zone and in the enargite zone. Birefringence seems to bear no relationship to compositional changes of either major or minor elements.

Limited microprobe analyses were conducted on a few grains of zunyite from two alunite-bearing samples, indicating chlorine contents of 2.65 to 3.4 wt percent.

Enargite zone

The enargite zone is best developed between grid lines 604 and 740, i.e., up to the central part of the former Principal pit at Colquijirca (Fig. 4). Between grid lines 644 and 684 mineralogical characterization is difficult because of pervasive overprinting of supergene mineralization, which is particularly well developed in this sector. The enargite zone displays the same mineral associations and assemblages as those observed in the enargite-gold zone but lacks discernible colusite, ferberite, or Au-bearing minerals. Other trace phases occurring as minuscule wisps within enargite, and more rarely, within pyrite I, are stibnite, emplectite, and small grains of unidentified bismuth-bearing minerals (microscopic observations tested via EDS tests).

At Colquijirca, enargite represents >95 vol percent of the copper phases in this zone. Luzonite is only locally as significant as in the Smelter deposit. The bulk of the enargite occurs cementing hydraulic breccias and incipient crackle breccias and in veinlets (Fig. 8A). Enargite forms typically massive aggregates, which under the microscope appear as mosaics of anhedral grains without any sign of development of crystal faces and showing abundant corrosion and recrystallization features. Again, as in the case of the enargite-gold zone at the Smelter deposit, an apparent relationship is observed between corrosion and recrystallization of enargite and the presence of alunite. In the enargite zone at Colquijirca most of the euhedral enargite is free of alunite and is mostly in contact with kaolinite and/or dickite (see below).

As in the enargite-gold zone, pyrite in the enargite zone (pyrite II) is volumetrically minor. Only north of grid line 700 is it up to 10 vol percent. Pyrite II typically occurs as euhedral pentagonal dodecahedral crystals up to 5 mm in size and accompanies alunite and fine-grained quartz but is free of enargite (Fig. 8C). Both pyrite II and fine-grained quartz II occur in direct contact with alunite without evidence of reaction and show reversed overgrowths with the latter mineral (Fig. 8D). The lack of apparent reaction is a significant difference from the fine-grained quartz I from the early quartz-pyrite stage and the coarse grains of quartz II simultaneously precipitated with enargite, which in places displays strong corrosion leaving only a skeletal vuggy mold. In general the alunite-quartz II-pyrite II assemblage overprints the quartz-pyrite replacement body. Detailed observation indicates that it extends slightly beyond the quartz-pyrite front, both along strike and across bedding (Fig. 9).

Alunite is distributed throughout the entire exposed enargite zone at Colquijirca, as an assemblage with fine-grained

TABLE 2. Representative Microprobe Analyses of Alunite from the Enargite-Gold, Enargite, and Sphalerite-Galena Zones

	Enargite-gold zone			Enargite zone			Sphalerite-galena zone	
Sample no.	PBR-130	PBR-131	PBR-338	PBR-298	PBR-218	PBR-322	PBR-108	PBR-253
K_2O	9.78	8.22	8.31	10.04	10.48	8.85	9.66	10.28
Na_2O	0.81	1.78	0.18	0.24	0.19	2.04	0.31	0.18
BaO	0.38	0.25	0.11	0.26	0.23	0.16	0.13	0.00
SrO	0.32	0.02	0.20	0.02	0.08	0.51	0.40	0.11
CaO	0.12	0.08	0.14	0.01	0.01	0.01	0.06	0.12
PbO	0.02	0.84	1.36	0.01	0.01	0.01	0.04	0.06
Al_2O_3	35.88	37.20	37.38	36.79	36.81	35.94	36.04	37.26
SO_3	39.90	38.86	38.63	39.01	38.35	40.84	39.28	39.53
P_2O_5	0.23	0.24	0.54	0.14	0.00	0.24	0.38	0.26
H_2O[2]	14.24	11.86	11.20	11.96	11.96	11.84	11.89	12.49
F^-	0.07	0.76	2.15	0.69	0.97	2.42	2.48	1.31
Total	101.75	100.11	100.19	99.17	99.08	102.86	100.67	101.61

[1] Alunites were analyzed using a Cameca SX50 electron microprobe at the University of Lausanne; instrumental conditions were: accelerating voltage of 12 kV, beam current of 10 nA, and spot size of 15 mm

[2] Wt percent H_2O calculated based on observed values of sulfur, phosphorous, potassium, sodium, strontium, barium, and fluorine, and alunite stoichiometry, using the formula $AR_3(SO_4)_2(F, OH)_6$, in which A refers to the large cations K^+, Na^+, Ba^{2+}, $Pb^{2+}$and Sr^{2+}, and R is Al^{3+}

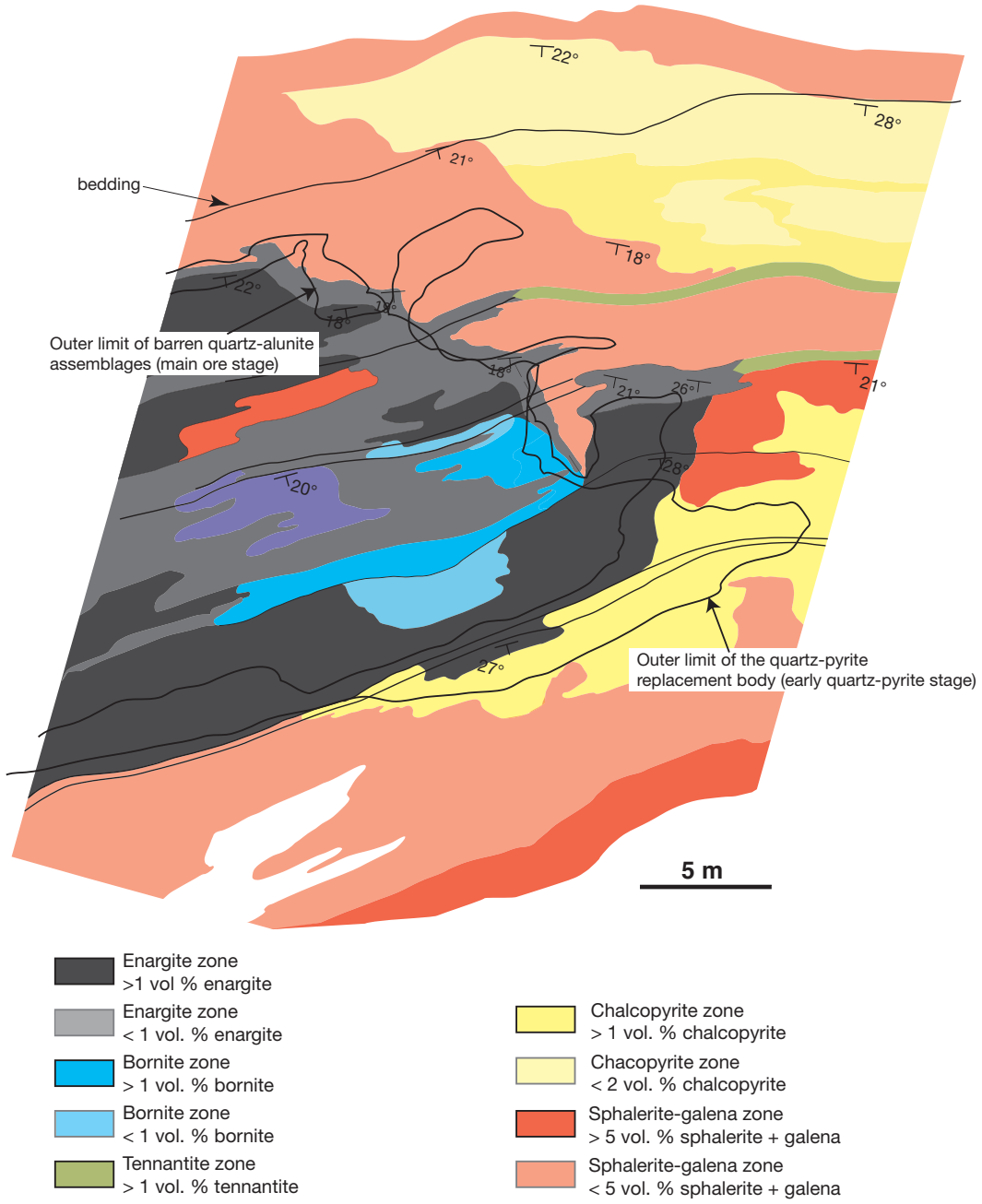

FIG. 9. Map of a portion of the transition sector between the enargite, bornite, tennantite, and chalcopyrite zones in the former Principal pit. The map is a projection of five benches on a vertical plan in a northeast-southwest direction (bedding dipping to the southeast). Also shown is the outer limit of the quartz-pyrite replacement body and external limit of the barren quartz-alunite-pyrite assemblage. The distribution of barren alunite-bearing assemblages differs from that of the enargite zone. Note the occurrence of enclave-like sphalerite-galena bodies in the copper zones. Approximate UTM coordinates of the center of the map: 8811296N, 361170E.

euhedral pyrite II with which it displays reversed overgrowths and intricate intergrowths. The alunite is typically platy and has a translucent whitish tone in contrast to that in the inner zones of the Smelter deposit. In comparison to the enargite-gold zone, alunite from the enargite zone is finer grained. Alunite typically fills intergranular spaces in enargite and quartz, both quartz I from the early quartz-pyrite stage and fine-grained quartz II. Detailed mapping shows that alunite-bearing assemblages are not restricted to the enargite zone but extend upward into the immediately overlying sphalerite-galena zone, where they coexist with sphalerite and galena (see below) and into the bornite zone (Fig. 9).

The absence of zunyite in the enargite zone is a significant difference between it and the enargite-gold zone. Kaolinite and dickite are common but minor phases with enargite.

Kaolinite and/or dickite occur in contact with euhedral enargite, commonly without any sign of corrosion or recrystallization, and fill intergranular spaces in enargite, as in much of the enargite-gold zone.

The enargite zone contains numerous lenses up to tens of centimeters thick of sphalerite-galena-pyrite-hematite-siderite-kaolinite. Crosscutting relationships indicate that this mineral association predates the enargite zone.

Gold-free tennantite-bearing associations are common in the enargite zone, particularly between grid lines 652 and 700 (Fig. 3). In places, in intervals up to several m thick, there is pervasive replacement of enargite by tennantite and to a lesser extent by chalcopyrite, bornite, and rare copper sulfosalts. The tennantite displays intricate intergrowths with these copper minerals. Thin sphalerite veins cutting enargite have been also observed in a few places (e.g., DDH CM-668, at 163 m).

Composition of minerals of the enargite zone: Except for alunite, no significant compositional variations were found in the main minerals of the enargite zone as compared to their compositions in the enargite-gold zone (Table A1). The composition approaches that of the alunite end member with Na/K ratios ranging typically from 0.03 to 0.08. No significant K substitution for Ca and Sr was found, and, in contrast to observations in the enargite-gold zone, virtually no Pb was found to occupy the A site of alunite from the enargite zone.

Bornite zone

The bornite zone occurs laterally in gradational contact with the enargite zone and is largely contained within the quartz-pyrite replacement. Observations in the Principal pit at Colquijirca show that over an interval of <60 cm bornite increases in volume and enargite is almost absent. The bornite zone has been identified only at Colquijirca but it presumably also occurs lateral to the enargite zone in the Smelter area; the wide spacing of drill holes does not allow confirmation of its presence in this area.

The bornite zone makes up no more than 2 vol percent of the global copper resources of the Smelter-Colquijirca mineralized corridor. It forms small discontinuous podlike bodies mostly near the front of the enargite zone (Fig. 9). These podlike bodies are up to 10 m long, 4 to 6 m wide, and 2 to 3 m thick. Copper grades are high, in places exceeding 5 wt percent, but because of its small tonnage the bornite zone is not mined for Cu. The main mineral association in this zone is bornite, tennantite, pyrite, quartz, barite, dickite, and kaolinite in addition to minor to trace quantities of sphalerite, covellite, chalcopyrite, chalcocite, digenite, galena, siderite, and a fine-grained mineral presumed to belong to the APS group. In this association, part of the pyrite, quartz, and sphalerite predate bornite deposition, whereas the rest of the minerals precipitated after the bornite.

The bornite typically occurs as irregular masses of anhedral grains. At microscopic scale the bornite displays abundant dissolution voids, mostly filled with dickite-(kaolinite; Fig. 10A) and, more rarely, with a finely crystallized mineral, presumably of the APS group. In most places, bornite grew interstitial to the matrix, which consists mostly of euhedral quartz with open-space filling textures. These textures show that bornite either coprecipitated with quartz or postdated it; bornite infillings within pyrite and barite are also observed.

Pyrite from the bornite zone is typically pentagonal dodecahedral (Fig. 10B), relatively coarse grained (up to 0.5 cm), and commonly occurs as clusters rimmed by bornite. In most examples, pyrite shows no reaction effects in contact with bornite (Fig. 10B), however, it is not rare to observe pyrite slightly to moderately replaced by bornite. Where bornite cements brecciated pyrite grains, which are angular and not resorbed, there is no reaction effect. Similarly, in bornite stockworks cutting euhedral pyrite, the pyrite fragments have matching contacts and do not show any evidence for reaction. A minor bornite fraction occurs as late wisps in this pyrite, partly filling minute fractures. Much of the sphalerite and quartz have a paragenetic position similar to or earlier than pyrite, showing no reaction where in contact with bornite. Sphalerite, extensively replaced by bornite, clearly predated this mineral (Fig. 10A). Chalcopyrite occurs as blebs within bornite or in some places as veinlets along its cleavage. Minor enargite occurs interstitial to quartz grains in an undefined temporal position relative to bornite. Mawsonite has been tentatively identified, based on its optical properties, between broken bornite fragments that display matching contacts. Bismuth-antimony-copper–bearing grains occurring as <10-μm blebs in pyrite, and locally in bornite, have been identified with EDS tests.

Quartz is abundant in the bornite zone, where it is typically euhedral and coarse grained (up to 1 cm). It may constitute up to >50 vol percent of the orebodies. The volumetrically most important (70–90%) type of quartz shows no evidence of reaction in contact with bornite and/or dickite-(kaolinite)-APS mineral. The second, less abundant type of quartz, shows significant corrosion where it is in contact with those minerals. Based on these relationships, it is considered that quartz precipitated both earlier than bornite and contemporaneous with or postdating it.

Barite accounts for between 1 and 5 vol percent of the bornite zone. It is typically coarse grained (0.5–2 cm) and shows two habits, both tabular. Predominantly, barite is dispersed through a mass of anhedral pyrite and/or bornite. Less commonly, barite occurs as overgrowths on pyrite and more rarely on bornite. Minute bornite inclusions in barite are common, suggesting that both minerals coprecipitated. As described above, kaolinite-(dickite) and a possible APS mineral typically fill vugs in bornite and quartz.

Limited microprobe analyses of bornite from the bornite zone are presented in Table A1. Sphalerite showing no reaction where in contact with bornite has FeS contents between 0.5 and 1.2 wt percent (Table 3).

Tennantite zone

A zone dominated by tennantite accompanied by major amounts of barite, pyrite, and quartz surrounds the bornite zone or in places occurs directly rimming the enargite zone. The tennantite zone has been identified northward from grid line 660 and is best developed in the Colquijirca deposit northward between grid lines 724 and 756 (Fig. 4). Minor phases of the tennantite zone include kaolinite, dickite, illite, smectite, enargite, chalcopyrite, bornite, stromeyerite, Bi-bearing sulfosalts, and numerous other sulfides and sulfosalts,

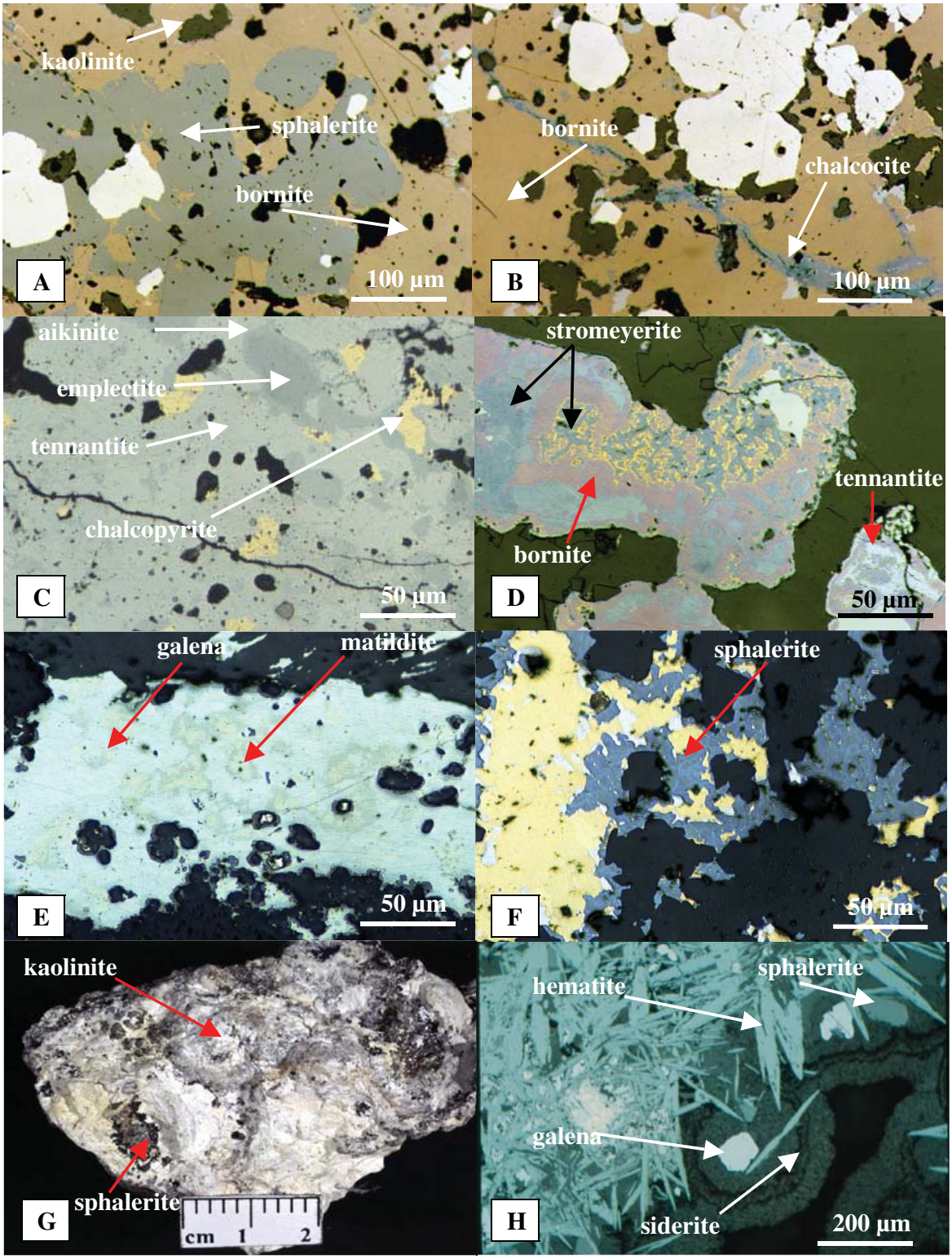

FIG. 10. Selected images of the bornite, tennantite, chalcopyrite, and sphalerite-galena zones. A. Reflected light microphotograph showing bornite (from the bornite zone) replacing sphalerite. Minor kaolinite filling voids. B. Same sample as in (A) in which bornite is cut by late ore-stage chalcocite. C. Sample from the tennantite zone containing several Bi-bearing minerals. D. Stromeyerite associated with chalcopyrite and partly replaced by chalcocite, and chalcopyrite rimming stromeyerite. E. Image from polished section of a sample rich in Ag and Bi. Matildite forms inclusions in galena. F. The sphalerite, chalcopyrite, galena, quartz association from the chalcopyrite zone. G. Nearly massive kaolinite sample containing euhedral sphalerite grains. H. Hematite accompanied by sphalerite, galena, and siderite of a typical ore sample from the external parts of the sphalerite-galena zone.

TABLE 3. Representative Analyses of Sphalerite in the Different Ore Zones Based on Electron Microprobe Analysis (wt %)

Sample	Ore zone	S	Zn	Fe	Cu	Total	FeS
PBR-148	Enargite-gold	32.73	66.33	0.05	0.09	99.20	**0.07**
PBR-148	Enargite-gold	32.73	66.74	0.02	0.15	99.63	**0.03**
PBR-148	Enargite-gold	32.42	66.43	0.04	0.13	99.02	**0.06**
MN-B	Bornite	32.37	65.60	0.29	0.50	98.76	**0.45**
MN-B	Bornite	32.33	65.83	0.54	0.65	99.35	**0.85**
MN-B	Bornite	32.48	65.01	1.06	1.04	99.59	**1.67**
MN-B	Bornite	32.54	65.62	0.84	0.72	99.72	**1.32**
MN-B	Bornite	32.67	65.22	0.88	0.85	99.62	**1.39**
PBR-287	Chalcopyrite	32.46	65.48	1.24	0.23	99.41	**1.95**
PBR-287	Chalcopyrite	32.86	64.82	1.04	0.66	99.38	**1.64**
PBR-287	Chalcopyrite	32.97	65.00	1.94	0.08	99.99	**3.06**
PBR-287	Chalcopyrite	33.01	65.03	1.92	0.08	100.04	**3.02**
PBR-287	Chalcopyrite	32.88	65.24	1.12	1.18	100.42	**1.76**
PBR-253	Sphalerite-galena (A)	32.89	66.87	0.08	0.33	100.17	**0.12**
PBR-253	Sphalerite-galena (A)	32.66	66.39	0.08	0.09	99.21	**0.12**
MN-F	Sphalerite-galena (K)	32.34	65.94	0.18	0.78	99.24	**0.28**
MN-F	Sphalerite-galena (K)	32.48	65.01	1.06	1.04	99.59	**1.67**
MN-F	Sphalerite-galena (K)	32.72	65.21	1.18	0.86	99.97	**1.86**
MN-H	Sphalerite-galena (SH)	32.87	64.23	1.20	0.96	99.26	**1.89**
MN-H	Sphalerite-galena (SH)	32.49	64.06	1.79	1.12	99.46	**2.82**
MN-H	Sphalerite-galena (SH)	32.24	61.80	2.41	2.87	99.32	**3.80**
MN-L	Sphalerite-galena (SM)	32.89	63.23	1.86	1.81	99.79	**2.93**
MN-L	Sphalerite-galena (SM)	32.66	60.84	3.42	1.86	98.78	**5.38**

Notes: Sphalerite was analyzed using a Cameca SX50 electron microprobe at the University of Lausanne; instrumental conditions were: accelerating voltage 15 kV, beam current 30 nA, and spot size of 10 um; Cd and Mn generally below detection limits; abbreviations: (A) = alunite-bearing subzone, (K) = kaolinite-dickite-bearing subzone, (SH) = siderite-bearing subzone and/or hematite-rich portions, (SM) = siderite-bearing subzone and/or magnetite-rich portions

only a few of them identified. Indeed, the tennantite zone is the most mineralogically complex of the whole Colquijirca district.

Typical grades in the tennantite zone are on the order of 1 to 2 wt percent Cu, 10 to 20 oz/t Ag (up to >100 oz/t), with variable, generally subeconomic amounts of Zn and Pb. The tennantite zone contains one of the three highest reported hypogene silver grades in the Colquijirca district. Although generally thin (at most 4 m thick and 6 m wide), its remarkable continuity (up to hundreds of meters surrounding the enargite zones and/or the bornite zones, even perpendicular to bedding) resulted in this zone being the most important silver source during the first three decades of the 20th century. In the tennantite-rich bodies exploited early in the 20th century, average mined grades fluctuated between 50 and 80 oz/t Ag (Lindgren, 1935; McKinstry, 1936). Pillars and other parts of these Ag-rich bodies have been intercepted in the former Principal pit. The particularly high silver contents in the Colquijirca deposit led several geologists during the 1920s and 1930s to study its ores in detail. It is presumed, based on mineralogy, that some of the rich ores studied by Orcel and Rivera Plaza (1920), McKinstry (1929, 1936), and Lindgren (1935) correspond to the tennantite zone.

A summary of the mineralogical characteristics of ores appearing to belong to the tennantite zone is based on the work cited above and confirmed by the present study. Orcel and Rivera Plaza (1920) described falhore (tennantite)-rich samples in which this mineral partially replaces skeletal pyrite; chalcopyrite inclusions in tennantite were also noted. These observations were confirmed in the present study. The classical paper by Lindgren (1935, p. 335) also describes tennantite-rich samples; in one he describes "a breccia of brown chert containing a little pyrite in minute grains; it is cemented by barite plates between which is abundant black tennantite in minute tetrahedrons." This type of tennantite-bearing sample is the most common in the tennantite zone. Druse- and geode-like cavities are common, formed by opening of fractures. Tennantite in open spaces, as described by Lindgren, occurs as euhedral tetrahedra, mostly no more than a few millimeters across. Barite in these samples has well-formed crystals, typically >1 cm wide, commonly twinned and translucent. Tennantite typically overgrows barite grains, but encapsulation of it and pyrite grains by barite are also common features. Lindgren (1935) also mentioned chalcopyrite replacing tennantite, and as well he recorded stromeyerite and a mineral that he deduced, from wet chemical analysis, to be emplectite. This is also a typical association of the tennantite zone.

Under the microscope, clusters of apparently monomineralic tennantite tetrahedra contain variable amounts of chalcopyrite, from traces to as much as 20 vol percent of the total copper-bearing phases (Fig. 10C). Chalcopyrite is also found along fractures and crystallographic planes. Less commonly, chalcopyrite occurs as open-space fillings and as rims on tennantite. Bornite is observed in the tennantite zone; some examples contain graticule-textured chalcopyrite similar texturally to exsolution products.

Stromeyerite commonly replaces tennantite and chalcopyrite. Another common habit of stromeyerite, as described by Lindgren (1935), is as rims on these last two phases, though particularly on chalcopyrite. The last association is also found in bornite-bearing samples of the tennantite zone, in which wisps of chalcopyrite occur within the bornite cleavage. Considerable amounts of bornite are found in parts close to the bornite zone, forming a sort of transition. Chalcopyrite rim-

ming stromeyerite in a mass of bornite has also been observed (Fig. 10D).

Emplectite is the most abundant accessory sulfosalt in the tennantite zone. It mostly occurs as minute inclusions in tennantite or rimming enargite blebs. Another uncommon mineral inclusion in tennantite appears to be aikinite, but its identification is not definitive (J. Injoque, pers. commun., 1988).

Native silver is relatively common in the tennantite zone, where it typically occurs growing on tennantite and/or barite. Several undefined argentiferous sulfur-bearing phases are spatially associated with this form of native silver. The very high silver contents (>40 oz/t Ag), and up to several hundreds oz/t in significant parts of the tennantite zone, are ascribed to associations containing stromeyerite, native silver, rare Ag-bearing sulfides and, in places, Ag-rich tennantite.

Barite is the most important associated gangue mineral in this zone. Besides clusters of perfectly formed and translucent tabular grains of museum quality, it occurs in a similar habit to that in the bornite zone. Minuscule tennantite inclusions in barite are common. Reversed crystallization between barite and tennantite is also observed. All these observations suggest that barite deposited coevally with tennantite.

Dickite and kaolinite may locally be important. The style is the same as that observed in the bornite zone, where these minerals fill all types of cavities. Where dickite and kaolinite are in contact with tennantite, neither corrosion nor recrystallization is observed.

Quartz in this zone is euhedral and relatively fine grained (< 5 mm in size). In contrast to quartz in the bornite zone, it is not a major component of the tennantite zone, with <5 vol percent of the minerals believed to have precipitated contemporaneously with tennantite. Reversed crystallization between quartz and tennantite may be distinguished in most samples, with both tennantite along the borders of quartz grains and quartz dispersed within masses of tennantite commonly observed. Another mineral, to date unidentified, occurs in pseudocubic crystals associated with quartz; it may be an APS mineral.

Composition of minerals of the tennantite zone: Microprobe analyses (Table A1) demonstrate that tennantite in the tennantite zone is largely stoichiometric (with <0.2 wt % Sb substituting for As) and that the compositions approximate those reported by Lindgren (1935) based on wet chemical analysis. In addition, the microprobe results confirm Lindgren's (1935) statement that the high contents of zinc and silver are true components in the tennantite structure and not derived from mixtures with other minerals. Zinc values are up to 9 wt percent, though Lindgren reported up to >12 wt percent. Silver has been found to be as high as 3.2 wt percent in tennantite (Table A1); however, in slight disagreement with the analytical results of Lindgren (1935), significant amounts of bismuth were found (up to 1.3 wt %). A few analyses of stromeyerite and emplectite are available in this study, with nearly perfect stoichiometry being found for all analyzed points in both cases (Table A2).

Chalcopyrite zone

A chalcopyrite-bearing zone extends for up to several hundred meters northward from grid line 660, along bedding as a thin rim to the tennantite zone, wider at the zoning front (Fig. 3). The chalcopyrite zone extends beyond the front of the main quartz-pyrite replacements and is best developed from approximately grid line 740 to 796 (Fig. 4). Besides chalcopyrite, this zone consists largely of pyrite, tennantite, sphalerite, galena, dickite, kaolinite, barite, quartz, siderite, and minor amounts of Bi- and Ag-bearing sulfosalts. Typical grades of the chalcopyrite zone are 0.2 to 0.5 percent Cu, 4.0 to 6.0 percent Zn, 2.0 to 3.0 percent Pb, and 3 to 5 oz/t Ag.

Pyrite is the main sulfide in the chalcopyrite zone and can attain >30 vol percent. An early pyrite generation is almost always partially replaced by chalcopyrite and occurs commonly associated with quartz in strongly silicified thin beds (<2 m thick). This early pyrite generation represents up to 90 vol percent of pyrite of the chalcopyrite zone. The stratigraphic position of these thin beds suggests that they constitute distal fingers of the early quartz-pyrite replacements. The second pyrite generation occurs intimately intergrown with chalcopyrite or as nearly euhedral grains disseminated in chalcopyrite matrix. No reaction is observed between this second pyrite generation (pyrite II) and chalcopyrite. Commonly, grains of this pyrite II occur broken in a matrix of chalcopyrite without discernible replacement.

Tennantite is the second most abundant copper mineral, typically occurring as tiny patches in chalcopyrite. Silver and Bi sulfosalts, in minor to trace quantities, are distributed throughout the chalcopyrite zone but are abundant in numerous small, elongated tabular bodies (5–20 m long, 1–3 m wide, and 1–2 m thick), mostly located in the central parts of the chalcopyrite zone. In addition to chalcopyrite and Ag and Bi sulfosalts these tabular bodies contain subordinate amounts of sphalerite and galena (Fig. 10F), the latter showing complex intergrowths, particularly with the sulfosalts suggesting coprecipitation. Typically, the small Ag- and Bi-bearing bodies grade 20 to 50 oz/t Ag, 1.0 to 3.0 percent Cu, and 0.5 to 1.0 percent Bi in addition to economically subordinate Zn and Pb (Zn + Pb <2 wt %). The main observed Ag and Bi hosts are matildite- and wittichenite-bearing assemblages (Fig. 10E). These assemblages are difficult to characterize due to their extremely fine grained character (<20 μm), but they seem to contain other much less abundant Ag- and Bi-bearing minerals. These Ag-Bi–rich bodies constitute the second bonanza-type silver ores mined underground during the early 20th century, when mined silver grades fluctuated between 50 and 80 oz/t Ag (Lindgren, 1935).

The chalcopyrite zone overprints numerous small (<20 m long, 2–5 m wide, and <2 m thick) tabular bodies rich in sphalerite and galena in addition to mainly siderite and kaolinite. Portions of the chalcopyrite zone, including in places overprinted sphalerite-galena bodies and high-grade Ag-Bi bodies, are the economically most valuable of the Colquijirca deposit; grades commonly average above 8.0 percent Zn, 3.0 Pb percent, 0.5 percent Cu, and 10 oz/t Ag. Mining of many of these small high-grade Ag-Bi bodies of the chalcopyrite zone allowed Sociedad Minera El Brocal S.A.A. to achieve the historical peak Ag production in 2006 of nearly 16 million ounces (Moz).

Dickite and subordinate kaolinite are the main gangue minerals in the chalcopyrite zone and together can amount up to more than 10 vol percent of the mineralized intervals. Typically, these clays occur filling open spaces between quartz,

sulfides, siderite, and barite and in no case is any sign of reaction observed. Breccia textures are a significant feature of the chalcopyrite zone, the most common one consisting of subangular silicified clasts in a silicified matrix partially replaced by chalcopyrite and pyrite. This matrix characterizes many of the small bodies enriched in Ag and Bi.

A selection of microprobe analyses of galena and chalcopyrite is given in Table A1. FeS contents of sphalerite range between 1 and 3 wt percent (Table 3); matildite analyses of a single sample are given in Table A4.

Sphalerite-galena zone

The sphalerite-galena zone mostly surrounds the chalcopyrite zone but in places it is observed to surround inner copper zones, including the enargite zone. In addition to sphalerite and galena it contains pyrite, quartz, alunite, kaolinite, dickite, Zn-bearing siderite, and hematite. The sphalerite-galena zone is best developed in the Colquijirca deposit between grid lines 700 and 780, where it constitutes the largest Zn-Pb-(Ag) resource of the deposit; prior to mining the zone may have exceeded 30 Mt at 6 percent Zn, 3 percent Pb, and 4 oz/t Ag. The sphalerite-galena zone extends north as far as grid line 828 at Condorcayán (Fig. 4) and also to the east, where at La Llave and La Pampa (Fig. 4) a large resource of nearly 47 Mt at 3.2 percent Zn, 1.1 percent Pb, and 1.4 oz/t Ag was recently defined (C. Yacila, pers. commun., 2008). This zone is also recognized east and west of the Smelter deposit, particularly northward from grid line 572 (Fig. 3).

The sphalerite-galena zone displays gradual changes in its mineralogical composition which from inner to outer positions show three main subzones consisting largely of (1) sphalerite, galena, pyrite, alunite, quartz, and barite; (2) sphalerite, galena, pyrite, dickite, kaolinite ± alunite, siderite, and (3) sphalerite, galena, siderite, hematite ± kaolinite.

The alunite-bearing subzone (subzone 1) occurs as small podlike bodies typically overlying the enargite zone, from grid lines 724 to 732. The alunite is intergrown with sphalerite, galena, barite, and quartz in druselike cavities cementing breccias or as coatings in small geodes in massive sphalerite-galena-pyrite bodies (Bendezú et al., 2008). Alunite blades commonly penetrate into pyrite, sphalerite, and galena, but neither sphalerite nor galena grains display signs of reaction when in contact with alunite and coarse-grained dickite. Sphalerite from this subzone varies in color from typically deep orange to yellow to in some cases colorless and is Fe poor (less than 0.1 wt % FeS; Table 3).

The kaolinite-dickite–bearing subzone is the most important volumetrically and occurs mainly surrounding the chalcopyrite zone between grid lines 740 and 796 (Fig. 4). Typically, this subzone contains at least 5 vol percent combined of kaolinite and dickite and locally up to more than 50 vol percent (Fig. 10G). Both kaolinite and dickite fill open spaces of sphalerite, galena, and pyrite clusters, and fine-grained sphalerite, galena, and pyrite occur as euhedral grains in a matrix of kaolinite. No evidence of corrosion or recrystallization of the sulfides is present. Siderite is a common minor mineral that occurs in massive replacements together with sphalerite, galena, and kaolinite; it shows neither dissolution nor recrystallization. In this kaolinite-dickite subzone there are meter-wide stratiform patches of a highly friable material called "sulfide rock" by the Colquijirca staff following an informal terminology (C. Yacila, pers. commun., 1998) for the main ores of the San Gregorio deposit south of the district. The sulfide rock has a microgranular texture (<100 μm) that gives the macroscopic appearance of an unconsolidated detrital rock. Sphalerite and galena occur generally intimately intergrown and displaying complex textures. Galena commonly replaces sphalerite, although sphalerite replacing galena is also observed. Sphalerite from the kaolinite-dickite subzone displays characteristically deep orange to yellowish to whitish internal reflections under crossed nicols and low FeS contents of ~0.1 to 0.5 wt percent (Table 3).

The siderite-hematite subzone contains, in addition to sphalerite and galena, considerable amounts of siderite, quartz, and hematite (Fig. 10H). Mine analyses and microprobe data reveal that the siderite may be significantly enriched in Zn. Typically, relatively coarse grained specular hematite occurs intergrown with this Zn-bearing siderite and minor kaolinite. As in the case of the kaolinite-dickite–bearing subzone, siderite in contact with kaolinite shows no evidence of dissolution or recrystallization. Magnetite commonly occurs partially replacing specular hematite and is most abundant in the external parts of the siderite-hematite subzone. Other characteristic but less abundant minerals from the siderite-hematite–bearing subzone include marcasite, quartz, fluorite, and fine-grained muscovite. Sphalerite from the siderite-hematite subzone is mostly brown and translucent, and FeS contents between 1 to 5 wt percent are the highest values found in the magnetite-bearing portions (Table 3).

The decreasing abundance of sphalerite relative to galena with increasing distance from the Cu-bearing zones is a remarkable feature of the sphalerite-galena zone. Thus, the alunite-bearing subzone contains on average 8 to 15 vol percent sphalerite and 3 to 5 vol percent galena (Sp/Gn: 3–4), the kaolinite-dickite subzone contains 5 to 8 vol percent sphalerite and 2 to 5 vol percent galena (Sp/Gn: 1–3), and the siderite-hematite–bearing subzone contains 2 to 5 vol percent sphalerite and 2 to 3 vol percent galena (Sp/Gn: 1–1.5). Dominance of galena over sphalerite is observed in external parts of the siderite-hematite subzone, including at La Pampa where several orebodies display an Sp/Gn ratio <1 (C. Yacila, pers. commun., 2008). Only galena is present in some of the outermost parts of the siderite-rich bodies.

Some small parts of the sphalerite-galena zone (<10 m long, <5 m wide, and <1 m thick) are Ag rich, as high as 30 to 50 oz/t. This occurs where galena predominates over sphalerite, and we presume that extremely fine grained Ag-bearing minerals occurring as inclusions in galena are the main silver minerals (likely argentite and acanthite). The distribution of old adits in several external parts of the sphalerite-galena zone, including those between grid lines 804 and 812 (Fig. 4), suggests that this ore type was also mined during the bonanza epoch at the beginning of the 20th century.

Zn-bearing carbonate zone

An outermost Zn-bearing carbonate zone surrounds the sphalerite-galena zone. In contrast to the other zones, it is virtually devoid of sulfides. This zone basically consists of Zn-bearing siderite and rhodochrosite and minor quartz in mantos less than 10 m long and wide and 3 m thick, with grades

commonly in the range of 1 to 5 wt percent Zn. The Zn-bearing carbonates occur mainly as patches that in places are massive. As a whole, the Zn-bearing carbonate zone can be depicted as a relatively homogeneous thin halo nearly completely surrounding the sphalerite-galena zone.

Barren outer zone

A barren zone consisting of calcite and subordinate dolomite patches and veinlets occurs above the entire Smelter-Colquijirca mineralized corridor and extends beyond the Zn-bearing carbonate zone. This spatial configuration suggests that the barren outer zone formed from spent main ore-stage fluids. Calcite veinlets have been recognized up to several hundreds of meters northward from the Zn-bearing carbonate zone and up to tens of meters above it. Recrystallization of carbonate rocks commonly accompanies the calcite and dolomite veining.

Late Ore Stage

The enargite-gold, enargite, and bornite zones from the main ore stage are overprinted by a late ore stage dominated by chalcocite with subordinated digenite and covellite and trace amounts of chalcopyrite. The late ore stage is structurally controlled underground in the Smelter deposit, where thin chalcocite veinlets tend to occur along northwest-trending subvertical faults and fractures. This late mineral stage has been recognized as deep as nearly 700 m below the oxidation zone (e.g., hole Brocal 524).

Most commonly the late ore stage is seen overprinting the enargite zones. Typically, chalcocite forms irregular poorly crystallized aggregates a few centimeters wide. Chalcocite replaces enargite along fractures and veinlets that continue into the main ore-stage minerals and may also replace pyrite II and late gold-bearing tennantite. Chalcocite is also observed coating pyrite II, and covellite and less commonly digenite may locally be as abundant as chalcocite. The last phases occur as fuzzy, fibrous aggregates with chalcocite or as rims to enargite grains.

Late ore stage chalcocite-(covellite-digenite) is also common in the bornite zone as thin veinlets <100 μm wide cutting bornite (Fig. 10). In a second form, these phases coat dissolution vugs. In both occurrences, chalcocite constitutes >50 vol percent of the mineral association, covellite constitutes between 10 and 40 vol percent, the remaining fraction being digenite and, subordinately, chalcopyrite. Locally there are pockets a few tens of centimeters across of massive chalcocite-(digenite-covellite-chalcopyrite).

Economically important late ore-stage chalcocite bodies were found in the Marcapunta Oeste project area (Vidal and Ligarda, 2004). The bodies appear, as at Smelter, to be structurally controlled by subvertical faults. In this area, chalcocite hosted by the Mitu Group red beds is commonly seen accompanied by appreciable amounts of fine-grained white muscovite in addition to unidentified phyllosilicates. In the Colquijirca deposit Ahlfeld (1932) noted that chalcocite is late and of hypogene origin. He described it replacing enargite in "the pyritic manto," very likely in the enargite zone.

Isotropic and stoichiometric chalcocite grains of the late ore stage overprint the enargite-gold zone. In contrast, chalcocite from the enargite zone between grid lines 660 and 692 is anisotropic in reflected light and shows Cu/S ratios mostly between 1.7 and 1.9.

Discussion and Interpretation

The geometry and mineralogical patterns of the early-stage quartz-pyrite replacements and main-stage orebodies provide insights into general features of the hydrothermal fluids that formed the Smelter-Colquijirca mineralized corridor. This discussion focuses on three aspects: controls of the flow movement, zoning, and variability of gangue mineralogy in the inner parts of the system.

The recognized geometric pattern, essentially derived from drill hole data, indicates that early fluids that formed the quartz-pyrite replacements migrated outward from the Marcapunta volcanic complex (Fig. 3). In the inner parts of the complex the fluids formed veins and, as they flowed upward and encountered a thick pile of carbonate rocks, mantos were formed roughly parallel to bedding and subordinate crosscutting structures were affected (Fig. 3). In the northern part of the district the fluids encountered the Pocobamba and Calera carbonate rocks and flowed northward along permeable beds; fluid flow was also controlled by northwest-southeast faults and folds at Smelter and by northeast-southwest faults and folds at Colquijirca (Figs. 3, 4). The main ore-stage fluids overprinted the quartz-pyrite replacement and continued to flow to the north. Orebodies largely adopted the morphology of the quartz-pyrite replacements and veins in the inner parts of Marcapunta and of the mantos within the Pocobamba and Calera sequences. Beyond the quartz-pyrite front, the main ore-stage fluids formed mantos controlled by the bedding of the Calera Formation (Fig. 4). A similar general longitudinal migration pattern is recorded in the southern sector of the district where the fluids seem to have been directed mainly by folds toward the Zn-Pb-(Ag) deposit of San Gregorio (Fig. 1).

Northward from grid line 580, the lithology of the sedimentary rocks exerted the main control on channeling the hydrothermal fluids responsible for the quartz-pyrite replacement. In addition, the quartz-pyrite replacement itself, which developed extensive intergrain microcavities (up to >1 mm wide), provided secondary permeability along which fluids flowed, enhancing the fluid migration. Fluids spread from permeable units into the immediately over- and underlying beds. At Colquijirca in the northern part of the mineralized corridor the common occurrence of mantos separated by barren intervals is due to relatively unreactive units such as massive argillites.

Folds also played an important role in channeling the ore fluids. Several large and rich bodies occur in the flexures of folds, including the Mercedes-Chocayoc orebody. They are comparable structurally to saddle-reef structures described in some vein deposits (e.g., Bendigo, Australia; e.g., Fowler and Winsor, 1997). This style of mineralization, controlled by bedding openings that result from flexure, is a typical feature of mineralization that postdates folding.

The characteristic well-developed zoning at Colquijirca is due to main ore-stage fluids that deposited mainly copper in the internal parts of the system and zinc and lead on the periphery. The mineral assemblages trace significant fluctuation

in terms of sulfidation state (Fig. 11). The change of high- to intermediate-sulfidation state is mainly recorded through internal zones outlined successively by enargite-pyrite–, bornite-pyrite–, and chalcopyrite-pyrite–bearing assemblages. Consistently, this decrease in sulfidation state is accompanied by an increase in FeS content in sphalerite, from less than 0.1 wt percent in the enargite zones to >5 wt percent in the outer parts of the sphalerite-galena zone implying a concomitant decrease in oxidation state. The decrease of sulfidation state is accompanied by an increase in pH as indicated by the nonopaque gangue mineralogy. Thus, the enargite-pyrite assemblages include commonly alunite and zunyite, whereas the chalcopyrite-pyrite assemblages contain abundant kaolinite, dickite, and siderite. The distribution of the kaolinite-bearing assemblages indicates that fluids were acidic during formation of the nearly entire sphalerite-galena and the Zn-bearing carbonate zones. Only at the leading edge of the system, where fluids were neutralized by the carbonate host rock, is near-neutral pH indicated by the precipitation of abundant calcite. In the outer parts of the system a decrease in the oxidation state of the fluids is recorded by the transition from hematite to magnetite.

Examination of crosscutting relationships on the basis of the described zoning model indicates that during the main ore stage, the inner Cu zones progressively overprinted the outer Zn-Pb zones, recording an advance of at least 1.5 km to the north for the mineralization front. The evidence for zonal growth in the Colquijirca district includes the numerous sphalerite-galena-siderite-hematite-kaolinite enclave-like bodies within the enargite-gold, enargite, and chalcopyrite zones. Similarly, the common occurrence in the enargite zones of hematite grains partly replaced by pyrite may represent remnants of the margins of the sphalerite-galena bodies (Fig. 8F). Also, much of the observed sphalerite and galena that predate copper minerals, mostly in the chalcopyrite zone, is best explained as residual assemblages from the sphalerite-galena zone (Fig. 10A).

The tennantite- and sphalerite-bearing associations that postdate enargite in the enargite zone are interpreted to represent retreat of the mineralization front. Most of the observations in which copper minerals from internal zones postdate those from external zones (e.g., chalcopyrite replacing tennantite, chalcopyrite veinlets cutting bornite) are consistent with a copper front retreating with time. Likewise, the widespread occurrence of magnetite replacing specular hematite in the

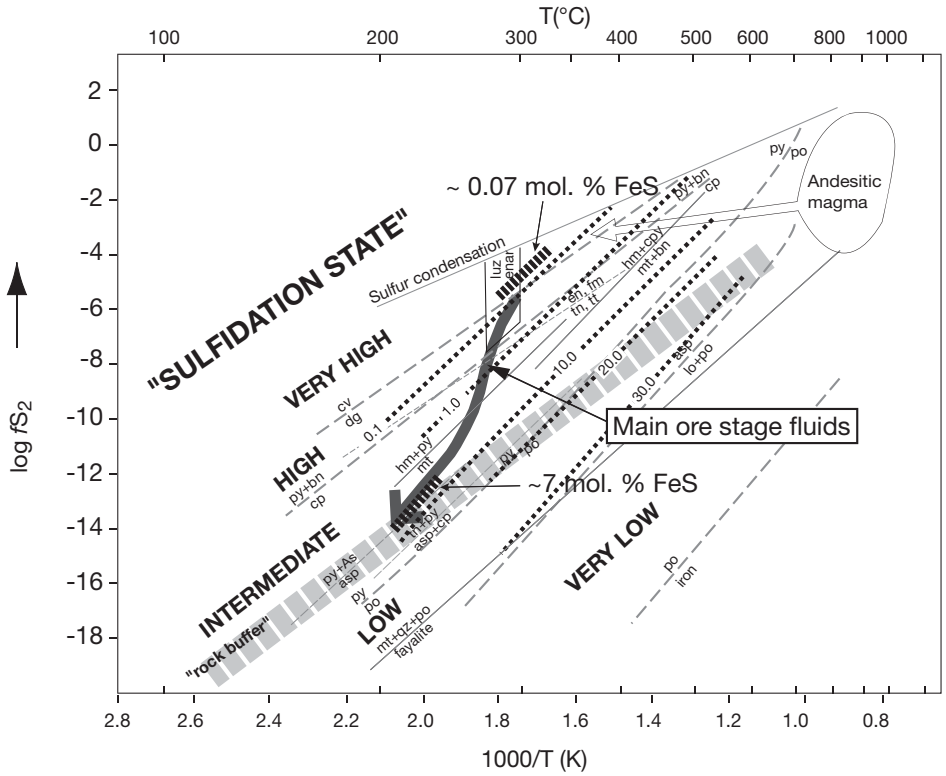

FIG. 11. Log f_{S_2} vs. T diagram, modified from Einaudi et al. (2003), illustrating the approximate cooling path of main ore-stage fluids based on observed mineral assemblages. A temperature of 300°C is assumed for the zunyite-bearing assemblages in the enargite-gold zone, 250°C for dickite-bearing assemblages in the chalcopyrite zone, and 200°C for the sphalerite-galena zones. These temperatures are consistent with those obtained from microthermometry reported by Bendezú (2007). Sulfidation reactions from Barton and Skinner (1979). Heavy dashed lines represent composition isopleths for sphalerite in equilibrium with either pyrite or pyrrhotite based on Czamanske (1974). Also shown are approximate contours of mole percent FeS for the two end-member Colquijirca sphalerites coexisting with pyrite. The cooling path of the main ore stage at Colquijirca is remarkably similar to that of stage II for Cerro de Pasco (Baumgartner et al., 2008) except for the widespread occurrence of famatinite-alunite assemblages in a significant part of the economical Zn-Pb-(Ag) mineralization at Cerro de Pasco, whereas at Colquijirca famatinite has only been identified locally at San Gregorio, in the southern part of the district.

sphalerite-galena zone probably indicates collapse of an external, less oxidized fluid that encroached onto an inner, more oxidized zone.

The advance and retreat of a mineralization front have been described and interpreted in detail elsewhere (e.g., Korzhinskii, 1946; Sales and Meyer, 1949). In the context of Cordilleran ore deposits, Sales and Meyer (1949) documented evidence for zone growth and retraction at the Butte deposit, and according to Einaudi (1982) and Einaudi et al. (2003), this constitutes a typical feature of zoned base metal veins. The observed geometry of the orebodies and mineralogical patterns at Colquijirca are consistent with the progressive shift of the whole zoned system.

The main ore-stage fluids, prior to significant interaction with the host rock, had high-sulfidation states as recorded by the internal enargite-bearing zones, in which the presence of alunite-zunyite reflects acidic conditions. Less acidic ore fluids result in the occurrence of smectite-illite and muscovite also in enargite-bearing assemblages. The common assemblages of kaolinite-dickite with enargite are intermediate in terms of acidity between the former two end members (Hemley and Jones, 1964). The distribution of the mineral assemblages and the crosscutting relationships indicate that variably acidic ore fluids as well as the fluids that formed the ore-free quartz-alunite assemblages likely entered the epithermal system as separate pulses.

According to fluid inclusion data (Bendezú, 2007), the acidic fluids that generated the quartz-alunite assemblages, both accompanied by base metal mineralization and devoid of it, were of low salinity, with typical values ranging from ~0 to ~3 percent NaCl equiv. These data suggest that the acidic fluids derived from a mixing process which involved variable amounts of two end-member fluids, one at 200° to 240°C with nearly zero salinities and the other at ~250° to 300°C and 3 to 4 percent NaCl equiv (Bendezú, 2007). Stable isotope O and H data from alunite (Bendezú, 2007) agree with this conclusion and define fluids with two contrasting compositional fields. The nil salinity fluid is characterized by a typical magmatic signature, whereas the saline fluid fits a meteoric water-magmatic water mixing trend. The nil salinity fluid was most likely a magmatic vapor plume, from which SO_2 condensed to form H_2SO_4, one of the main acids responsible for the formation of the quartz-alunite alteration. Sulfur isotope compositions of alunite (Bendezú, 2007) support this origin, in which sulfate has equilibrated with H_2S formed through disproportionation of SO_2 within a condensing vapor plume (e.g., Rye, 1993).

Our preferred interpretation of the significant fluctuations in the acidity of the ore fluids involves mixing between vapor condensates rich in HCl and sulfate and less acidic low- to moderate-saline ore-forming fluids (derived from single-phase fluid of intermediate density in the sense of Hedenquist et al. (1998) or from brines diluted by meteoric waters). Figure 12 illustrates this scenario: (A) strongly acidic ore fluids resulting from mixing of magmatic vapor-derived acidic fluids with low- to moderate-salinity fluids of magmatic origin; (B) weakly acidic ore fluids with a moderate to small component of magmatic vapor-derived acidic fluids. There is also the situation (C) in which only barren acidic fluids derived from magmatic-vapor enter the epithermal environment. In situation (D), which may be important in districts other than Colquijirca, low- to moderate-salinity ore fluids of magmatic origin enter the epithermal environment without mixing with the magmatic vapour-derived acidic fluids.

The Cordilleran ores at Colquijirca can be explained mainly by case (A), whereas cases (B) and (D) may explain weakly zoned Zn-Pb-(Ag-Cu) mineralization parts of Cerro de Pasco (Baumgartner et al., 2008), Domo de Yauli (Beuchat et al., 2004), Morococha (Catchpole et al., 2008), and elsewhere. It is postulated that formation of strongly zoned Cordilleran deposits depends on the availability of magmatic vapor-bearing SO_2, HCl, and other strong acids which, in addition to emplacement constraints, are ultimately related to the nature of the parental magma.

Conclusions

The detailed study of Colquijirca has documented one of the best-known examples of zoned epithermal polymetallic mineralization. The mineralogical patterns of the Smelter-Colquijirca corridor indicate that the sulfide-rich Cu-Zn-Pb-(Au-Ag) mineralization of the northern part of the Colquijirca district is the result of superimposition of three main stages. During an early quartz-pyrite stage in which no economic ore was deposited, carbonate rocks surrounding the Marcapunta diatreme-dome complex were replaced by quartz and pyrite. The economically important main ore stage followed, largely superimposed on most of the quartz-pyrite replacements; this stage produced the strong zoning observed along much of the Smelter-Colquijirca corridor. A late ore stage deposited chalcocite, mostly overprinting the various Cu-bearing zones of the main ore stage. The sequence and mineralogy of these stages are comparable to those observed in late veinlets in numerous porphyry copper deposits (e.g., Gustafson and Hunt, 1975; Einaudi, 1982; Seedorff et al., 2005) and is consistent with the hypothesis that Cordilleran mineralization formed late in the hydrothermal history of porphyry copper systems, typically on their distal margins (Bendezú et al. 2003, 2008).

The process of advancement and retraction of the whole mineralized system is a major part of forming Cordilleran ore deposits and is mainly responsible for their mineralogical complexity and complex crosscutting relationships, as observed in much of the Colquijirca district.

Significant fluctuations in the acidity of the ore fluids in the central parts of the system are interpreted in terms of mixing between variable amounts of acidic oxidized vapor condensates and less acidic low- to moderate-salinity fluids of magmatic derivation.

Acknowledgments

This project was supported by the Swiss National Science Foundation (NSF) grant 2000-062000.00. We thank Sociedad Minera El Brocal S.A.A. for logistical support and for permission to publish this paper. We wish to thank Carlos Yacila, Ivan Monteagudo, Lucio Canchis, and Máximo Yaringano, former Colquijirca geologists, for valuable discussions, particularly during the early stage of this work. Richard Sillitoe's revision of an earlier version of this manuscript when it was part of a Ph.D. thesis by the senior author and his encouragement to publish a paper with this descriptive character is much appreciated. We also thank Noel White and Jeff Hedenquist for their careful review with numerous suggestions, as well as

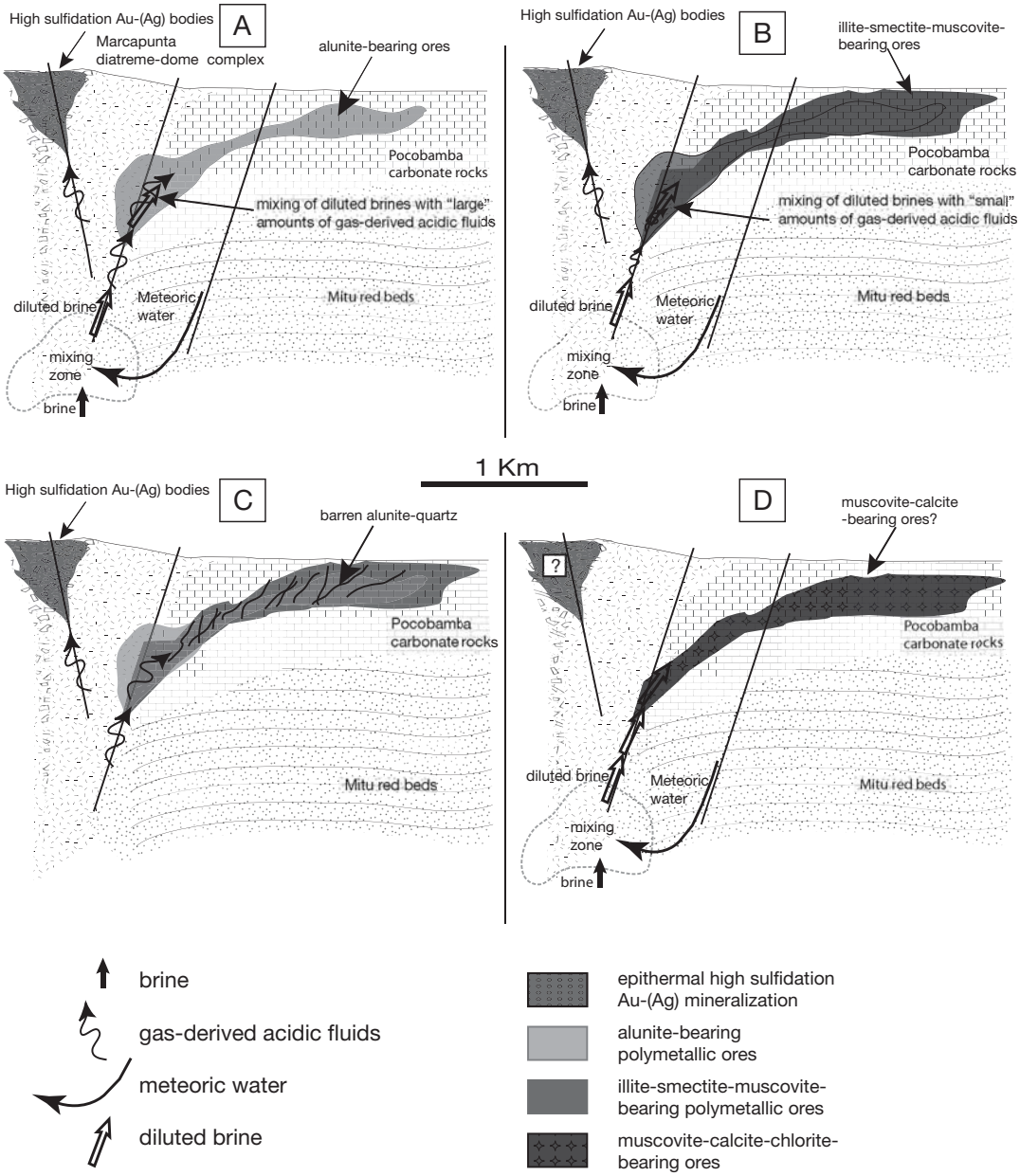

FIG. 12. Proposed scenarios of generation of variably acidic ore fluids from mixing between vapor condensates rich in HCl and sulfate and less acidic low- to moderate-saline ore-forming fluids (derived from single phase fluid of intermediate density in the sense of Hedenquist et al. (1998) or from brines diluted by meteoric waters). A. Strongly acidic ore fluids resulting from mixing of magmatic vapor-derived acidic fluids with low- to moderate-salinity fluids of magmatic origin. B. Weakly acidic ore fluids with a moderate to small component of magmatic vapor-derived acidic fluids. C. Only barren acidic fluids derived from magmatic-vapor enter the epithermal environment and superimpose on the ores. In situation (D), which may be more important in other districts than in Colquijirca, low- to moderate-salinity ore fluids (D) of magmatic origin enter the epithermal environment without mixing with the magmatic-vapor–derived acidic fluids.

Antonio Arribas, Benoit Dube, and Larry Meinert for their reviews and comments.

REFERENCES

Ahlfeld, F., 1932, Die Silberlagerstätte Colquijirca, Perú: Zeitschrift Praktischer Geologie, v. 40, p. 81–87.

Alvarez, A.A., and Noble, D.C., 1988, Sedimentary rock-hosted disseminated precious metal mineralization at Purísima Concepción, Yauricocha district, central Peru: ECONOMIC GEOLOGY, v. 83, p. 1368–1378.

Angeles, C., 1999, Los sedimentos Cenozoicos de Cerro de Pasco: Estratigrafia, sedimentación y tectónica: Sociedad Geológica del Perú, v. 5, p. 103–118.

Barton, P.B., Jr., 1970, Sulfide petrology: Mineralogical Society of America Special Paper 3, p. 187–198.

Barton, P.B., Jr., and Skinner, B.J., 1979, Sulfide mineral stabilities, *in* Barnes, H. L., ed., Geochemistry of hydrothermal ore deposits, 2nd ed.: New York, Holt, John Wiley and Sons, p. 278–403.

Barton, P.B.J., Bethke, P.M., and Toulmin, P.I., 1963, Equilibrium in ore deposits: Mineralogical Society of America Special Paper 1, p. 171–185.

Bartos, P.J., 1989, Prograde and retrograde base metal lode deposits and their relationship to underlying porphyry copper deposits: Economic Geology, v. 84, p. 1671–1683.

Baumgartner, R., Fontboté, L., and Vennemann, T., 2008, Mineral zoning and geochemistry of epithermal polymetallic Zn-Pb-Ag-Cu-Bi mineralization at Cerro de Pasco, Peru: Economic Geology, v. 103, p. 493–537.

Bendezú, R., 1997, Características geológicas mineralógicas y geoquímicas de los yacimientos de Zn-Pb (±Ag) de San Gregorio y Colquijirca emplazados en unidades sedimentarias en los bordes del sistema epitermal de alta sulfuración de Marcapunta: Unpublished M.Sc. thesis, Lima, Universidad Nacional de Ingeniería, 60 p.

——2007, Shallow polymetallic and precious metal mineralization associated with a Miocene diatreme-dome complex: The Colquijirca district of the Peruvian Andes, Geneva, Switzerland, University of Geneva, Terre & Environnement, v. 64, 221 p.

Bendezú, R., Fontboté, L., and Cosca, M., 2003, Relative age of Cordilleran base metal lode and replacement deposits, and high sulfidation Au-(Ag) epithermal mineralization in the Colquijirca mining district, central Peru: Mineralium Deposita, v. 38, p. 683–694.

Bendezú, R., Page, L., Spikings, R., Pecskay, Z., and Fontboté, L., 2008, New $^{40}Ar/^{39}Ar$ alunite ages from the Colquijirca district, Peru: Evidence of a long period of magmatic SO_2 degassing during formation of epithermal Au-Ag and Cordilleran polymetallic ores: Mineralium Deposita, v. 43, p. 777–789.

Beuchat, S., Moritz, R., and Pettke, T., 2004, Fluid evolution in the W-Cu-Zn-Pb San Cristobal vein, Peru: Fluid inclusion and stable isotope evidence: Chemical Geology, v. 210, p. 201–224.

Catchpole H., Bendezú A., Kouzmanov K., Fontboté L., and Escalante E., 2008, Porphyry- related base metal mineralization styles in the Miocene Morococha district, central Peru: Society of Economic Geologists-Geological Society of South Africa 2008 Conference, Johannesburg, July 05–06, 2008, Programs and Abstracts, p. 54–57.

Czamanske, G.K., 1974, The FeS content of sphalerite along the chalcopyrite-pyrite-bornite sulfur fugacity buffer: Economic Geology, v. 69, p. 1328–1334.

Einaudi, M.T., 1968, Copper zoning in pyrite from Cerro de Pasco, Perú: American Mineralogist, v. 53, p. 1748–1752.

——1982, Description of skarns associated with porphyry copper plutons, *in* Titley, S., ed., Advances in geology of the porphyry copper deposits southwestern North America: Tucson, AZ, University of Arizona Press, p. 139–183.

Einaudi, M.T., Hedenquist, J.W., and Inan, E., 2003, Sulfidation state of fluids in active and extinct hydrothermal systems: Transitions from porphyry to epithermal environments: Society of Economic Geologists and Geochemical Society Special Publication 10, p. 285–313.

Farfán Bernales, C., 2006, Modelo de Prospección Geológica de Yacimientos Minerales en Rocas Carbonatadas, Región de Pasco-Mina Vinchos: Unpublished M.Sc. thesis, Lima, Peru, Universidad National Mayor San Marcos, 50 p.

Fontboté, L., and Bendezú, R., 2009, Cordilleran or Butte-type veins and replacement bodies as a deposit class in porphyry systems: Society of Geology Applied to Ore Deposits Meeting, 10th Biennial,Townsville, Australia, Proceedings, p. 521–523.

Fowler, T.J., and Winsor, C.N., 1997, Characteristics and occurrence of bedding-parallel slip surfaces and laminated veins in chevron folds from the Bendigo-Castlemaine goldfields: Implications for flexural slip folding: Journal of Structural Geology, v. 19, p. 799–815.

Guilbert, J.M., and Park, J.R., 1986, The geology of ore deposits: New York, Freeman and Co., 750 p.

Gustafson, L., and Hunt, J.P., 1975, The porphyry copper deposit at El Salvador, Chile: Economic Geology, v. 70, p. 857–912.

Hedenquist, J.W, Arribas A.J, and Reynolds T.J., 1998, Evolution of an intrusion-centered hydrothermal system: Far Southeast-Lepanto porphyry and epithermal Cu-Au deposits, Philippines: Economic Geology, v. 93, p. 373–404.

Hemley, J.J., and Hunt, J.P., 1992, Hydrothermal ore-forming processes in the light of studies in rock-buffered systems: II. Some general geologic applications: Economic Geology, v. 87, p. 23–43.

Hemley, J.J., and Jones, W.R., 1964, Chemical aspects of hydrothermal alteration with emphasis on hydrogen metasomatism: Economic Geology, v. 59, p. 538–569.

Jenks, W.F., 1951, Triassic to Tertiary stratigraphy near Cerro de Pasco, Peru: Geological Society of America Bulletin, v. 62, p. 203–219.

Kamilli, R.J., and Ohmoto, H., 1977, Paragenesis, zoning, fluid inclusion, and isotopic studies of the Finlandia vein, Colqui district, central Peru: Economic Geology, v. 72, p. 950–982.

Korzhinskii, D.S., 1946, Metasomatic zonation near fractures and veins: Zapiski of All-Union Mineralogical Society (ZVMO), v. 75, p. 321–332 (in Russian).

Kouzmanov, K., Ovtcharova, M., von Quadt, A., Guillong, M., Spikings, R., Schaltegger, U., Fontboté, L., and Rivera, L., 2008, U-Pb and $^{40}Ar/^{39}Ar$ constraints for the timing of magmatism and mineralization in the giant Toromocho porphyry Cu-Mo deposit, central Peru: Congreso Peruano de Geologia, 14th, Lima, Peru, Proceedings.

Lindgren, W., 1935, The silver mine of Colquijirca, Perú: Economic Geology, v. 30, p. 331–346.

Macfarlane, A.W., Marcet, P., LeHuray, A.P., and Petersen, U., 1990, Lead isotope provinces of the Central Andes inferred from ores and crustal rocks: Economic Geology, v. 85, p. 1857–1880.

Manske, S.L., and Paul, A.H., 2002, Geology of a major new porphyry copper center in the Superior (Pioneer) district, Arizona: Economic Geology, v. 97, p.197–220.

McKinstry, H.E., 1929, Interpretation of concentric textures at Colquijirca, Perú: American Mineralogist, v. 14, p. 431–433.

——1936, Geology of the silver deposit at Colquijirca, Perú: Economic Geology, v. 31, p. 619–635.

McLaughlin, D.H., 1924, Geology and physiography of the Peruvian Cordillera, Department of Junin and Lima: Geological Society of America Bulletin, v. 35, p. 591–632.

Noble, D.C., and McKee, E.H., 1999, The Miocene metallogenic belt of central and northern Perú: Society of Economic Geologists Special Publication 7, p. 155–193.

Orcel, J., and Rivera Plaza, G., 1920, Etude microscopique de quelques minerais métalliques du Pérou: Bulletin Societé Française de Minéralogie, v. 52, p. 91–107.

Ramdohr, P., 1980, The ore minerals and their intergrowths: Heidelberg, Pergamon Press, 1207 p.

Rye R.O., 1993, The evolution of magmatic fluids in the epithermal environment—the stable isotope perspective: Economic Geology, v. 88, p.733–752.

Sales, R.H., and Meyer, C., 1949, Results from preliminary studies of vein formation at Butte, Montana: Economic Geology, v. 44, p. 465–484.

Sarmiento, J., 2004, Domos de lava relacionadas a la diatrema principal en centro volcánico Marcapunta, Distrito Minero de Colquijirca-Peru Central: Unpublished M.Sc. thesis, Universidad Nacional San Antonio Abad del Cuzco, 86 p.

Sawkins, F.J., 1972, Sulfide ore deposits in relation to plate tectonics: Journal of Geology, v. 80, p. 377–397.

Seedorff, E., Dilles, J.H., Proffett, J.M., Jr., Einaudi, M.T., Zurcher, L., William J. A. Stavast, W. J.A., Johnson, D.A., and Barton, M.D., 2005, Porphyry-related deposits: Characteristics and origin of hypogene features: Economic Geology 100th Anniversary Volume, p. 251–298.

Vidal, C., and Ligarda, R., 2004, Enargite-gold deposits at Marcapunta, Colquijirca mining district, central Perú: Mineralogic and geochemical zoning in subvolcanic, limestone-replacement deposits of high-sulfidation epithermal type: Society of Economic Geology Special Publication 11, p. 231–242.

Vidal, C., Mayta, O., Noble, D.C., and McKee, E.H., 1984, Sobre la evolución de las soluciones hidrotermales dentro del centro volcánico Marcapunta en Colquijirca-Pasco: Volumen Jubilar Sociedad Geológica del Perú, v. 10, p. 1–14.

Vidal, C., Proaño, J., and Noble, N., 1997, Geología y distribución hidrotermal de menas con Au, Cu, Zn, Pb y Ag en el Distrito Minero Colquijirca, Pasco: Congreso Peruano de Geología, 9th, Lima, Proceedings, p. 217–219.

TABLE A1. Typical Compositions of Major Sulfur-Bearing Phases from the Main Ore Stage Based on Electron Microprobe Analysis

Sample	Mineral	Stage/zone	S	Fe	Cu	As	Ag	Sb	Bi	Sn	Zn	Pb	Total
PBR-132	Pyrite I	Early quartz-pyrite stage	54.40	46.02	0.09	0.12	0.01	0.01	n.d.	n.d.	n.a.	n.a.	100.54
PBR-132	Pyrite I	Early quartz-pyrite stage	54.77	45.94	0.19	0.04	0.01	n.d.	n.d.	n.d.	n.a.	n.a.	100.95
PBR-137	Pyrite I	Early quartz-pyrite stage	54.35	45.43	0.08	0.08	0.01	n.d.	0.11	0.02	n.a.	n.a.	99.98
PBR-137	Pyrite I	Early quartz-pyrite stage	54.02	45.16	0.17	0.01	0.01	n.d.	n.d.	0.01	n.a.	n.a.	99.36
PBR-391	Pyrite II	Main ore stage/EGZ	54.72	46.07	0.54	0.07	0.02	0.05	n.d.	n.d.	n.a.	n.a.	101.47
PBR-391	Pyrite II	Main ore stage/EGZ	54.85	45.76	0.31	0.12	n.d.	n.d.	n.d.	n.d.	n.a.	n.a.	100.94
PBR-247	Pyrite II	Main ore stage/EGZ	54.68	45.71	0.32	0.21	0.01	n.d.	n.d.	n.d.	n.a.	n.a.	100.72
PBR-247	Pyrite II	Main ore stage/EGZ	54.66	45.88	0.41	0.13	0.02	n.d.	0.02	0.02	n.a.	n.a.	101.05
PBR-132	Enargite	Main ore stage/EGZ	32.64	0.06	49.27	17.68	n.d.	0.42	n.d.	0.08	n.a.	n.a.	100.08
PBR-132	Enargite	Main ore stage/EGZ	32.12	0.05	49.65	18.22	n.d.	0.27	n.d.	0.18	n.a.	n.a.	100.32
PBR-132	Enargite	Main ore stage/EGZ	33.36	n.d.	48.88	17.32	0.09	0.26	n.d.	0.67	n.a.	n.a.	99.91
PBR-263	Enargite	Main ore stage/EGZ	33.08	0.01	49.02	17.11	0.03	0.89	n.d.	0.23	n.a.	n.a.	100.14
PBR-263	Enargite	Main ore stage/EGZ	32.98	n.d.	49.22	17.07	0.03	0.83	n.d.	0.26	n.a.	n.a.	100.13
PBR-263	Enargite	Main ore stage/EGZ	32.77	0.03	48.59	17.01	0.09	0.81	n.d.	0.43	n.a.	n.a.	99.29
PBR-265	Enargite	Main ore stage/EGZ	33.19	0.02	48.82	17.22	0.07	0.50	n.d.	0.27	n.a.	n.a.	99.82
PBR-265	Enargite	Main ore stage/EGZ	33.20	0.10	49.27	17.67	0.07	0.02	0.20	n.d.	n.a.	n.a.	100.33
PBR-265	Enargite	Main ore stage/EGZ	33.25	0.12	48.66	17.38	0.11	0.44	n.d.	0.47	n.a.	n.a.	99.96
PBR-137	Enargite	Main ore stage/EGZ	33.11	0.27	48.87	17.67	0.05	0.10	n.d.	0.04	n.a.	n.a.	100.07
PBR-137	Enargite	Main ore stage/EGZ	33.21	0.27	49.02	17.72	0.05	0.10	0.01	0.04	n.a.	n.a.	100.37
PBR-137	Enargite	Main ore stage/EGZ	33.31	0.27	49.17	17.77	0.05	0.10	0.01	0.04	n.a.	n.a.	100.68
PBR-132	Luzonite	Main ore stage/EGZ	32.97	0.94	47.78	16.25	n.d.	1.16	n.d.	1.61	n.a.	n.a.	99.10
PBR-132	Luzonite	Main ore stage/EGZ	32.34	n.d.	49.03	17.04	0.01	1.81	n.d.	0.06	n.a.	n.a.	100.24
PBR-265	Luzonite	Main ore stage/EGZ	33.03	1.09	47.19	16.37	0.10	1.24	n.d.	0.91	n.a.	n.a.	99.01
PBR-265	Luzonite	Main ore stage/EGZ	33.36	1.10	47.66	16.53	0.10	1.25	n.d.	0.76	n.a.	n.a.	100.00
PBR-132	Colusite	Main ore stage/EGZ	30.60	0.64	54.25	7.41	n.d.	0.02	n.d.	7.03	n.a.	n.a.	99.95
PBR-131	Colusite	Main ore stage/EGZ	29.81	2.74	52.25	4.82	n.d.	n.d.	0.02	10.96	n.a.	n.a.	100.61
PBR-131	Colusite	Main ore stage/EGZ	30.85	0.59	54.51	8.10	n.d.	n.d.	n.d.	6.55	n.a.	n.a.	100.59
PBR-131	Colusite	Main ore stage/EGZ	30.62	0.86	52.37	8.32	n.d.	0.02	0.01	7.34	n.a.	n.a.	99.54
PBR-218	Pyrite II	Main ore stage/EZ	54.71	45.48	0.04	0.02	0.04	n.d.	n.d.	n.d.	n.a.	n.a.	100.27
PBR-218	Pyrite II	Main ore stage/EZ	54.40	46.22	0.09	0.12	0.01	0.01	n.d.	n.d.	n.a.	n.a.	100.84
PBR-218	Pyrite II	Main ore stage/EZ	54.35	45.43	0.08	0.08	0.01	n.d.	0.11	0.02	n.a.	n.a.	100.08
PBR-244	Pyrite II	Main ore stage/EZ	54.02	45.16	0.17	0.01	0.01	n.d.	n.d.	0.01	n.a.	n.a.	99.37
PBR-244	Pyrite II	Main ore stage/EZ	53.70	45.89	0.16	0.08	0.01	n.d.	n.d.	n.d.	n.a.	n.a.	99.84
PBR-244	Pyrite II	Main ore stage/EZ	53.38	45.62	0.16	0.12	0.01	n.d.	n.d.	n.d.	n.a.	n.a.	99.29
PBR-218	Enargite	Main ore stage/EZ	32.64	0.06	49.27	17.68	n.d.	0.42	n.d.	0.08	n.a.	n.a.	100.16
PBR-218	Enargite	Main ore stage/EZ	32.55	0.25	48.49	17.33	n.d.	0.45	n.d.	0.00	n.a.	n.a.	99.07
PBR-218	Enargite	Main ore stage/EZ	32.89	0.05	48.66	16.80	0.31	0.74	n.d.	0.30	n.a.	n.a.	99.76
PBR-244	Enargite	Main ore stage/EZ	33.18	0.05	48.36	17.11	0.10	0.40	0.25	0.34	n.a.	n.a.	99.79
PBR-244	Enargite	Main ore stage/EZ	33.08	0.01	49.02	17.11	0.03	0.89	n.d.	0.23	n.a.	n.a.	100.37
PBR-244	Enargite	Main ore stage/EZ	32.77	0.03	48.59	17.01	0.09	0.81	n.d.	0.43	n.a.	n.a.	99.72
PBR-187	Bornite	Main ore stage/BZ	25.37	11.18	64.06	0.03	0.01	0.02	n.a.	0.11	n.a.	n.d.	100.78
PBR-187	Bornite	Main ore stage/BZ	25.89	11.21	64.07	0.07	0.01	0.02	n.a.	0.14	n.a.	n.d.	0.00
PBR-187	Bornite	Main ore stage/BZ	25.26	11.04	64.55	0.01	0.01	0.01	n.a.	0.11	n.a.	n.d.	0.00
PBR-187	Bornite	Main ore stage/BZ	25.26	11.20	64.65	0.03	0.12	0.05	n.a.	0.04	n.a.	n.d.	101.35
PBR-95	tennantite	Main ore stage/TZ	28.22	3.33	46.13	18.77	0.01	0.83	n.d.	0.15	3.91	n.d.	0.00
PBR-95	tennantite	Main ore stage/TZ	28.38	6.02	46.57	19.47	n.d.	0.06	n.d.	n.d.	0.02	n.d.	0.00
PBR-95	tennantite	Main ore stage/TZ	28.21	4.22	45.26	18.84	0.04	0.12	n.d.	0.08	3.11	n.d.	0.00
PBR-95	tennantite	Main ore stage/TZ	28.44	3.78	44.54	18.26	0.04	0.40	n.d.	0.41	3.51	n.d.	0.00
PBR-123	Chalcopyrite	Main ore stage/CHZ	34.63	29.50	34.74	0.03	0.06	0.07	0.09	0.03	n.d.	n.d.	0.00
PBR-123	Chalcopyrite	Main ore stage/CHZ	34.37	29.93	34.65	0.01	n.d.	n.d.	n.d.	0.06	0.14	n.d.	0.00
PBR-123	Chalcopyrite	Main ore stage/CHZ	34.71	29.90	34.63	0.03	0.01	n.d.	n.d.	0.04	0.16	n.d.	0.00
PBR-123	Chalcopyrite	Main ore stage/CHZ	34.44	29.43	34.56	0.02	0.03	0.05	n.d.	0.06	0.32	n.d.	0.00
MN-A	Galena	Main ore stage/SGZ	13.50	0.18	0.46	0.01	0.03	0.01	n.d.	0.03	0.34	86.27	0.00
MN-A	Galena	Main ore stage/SGZ	13.41	0.53	1.02	n.d.	0.41	0.01	n.d.	0.05	0.29	85.10	0.00
MN-A	Galena	Main ore stage/SGZ	13.07	0.05	0.24	0.01	0.07	n.d.	n.d.	0.02	0.28	86.81	0.00
MN-C	Galena	Main ore stage/SGZ	13.30	n.d.	0.16	n.d.	n.d.	n.d.	n.d.	n.d.	0.91	86.25	0.00
MN-C	Galena	Main ore stage/SGZ	13.40	0.03	n.d.	0.02	n.d.	0.02	n.d.	0.07	0.08	86.08	0.00
MN-C	Galena	Main ore stage/SGZ	13.21	0.05	0.04	n.d.	n.d.	n.d.	n.d.	0.02	n.d.	86.78	0.00
MN-C	Galena	Main ore stage/SGZ	13.08	0.02	0.03	n.d.	n.d.	n.d.	n.d.	0.03	0.04	86.23	0.00

Sulfides and sulfosalts were analyzed using a Cameca SX50 electron microprobe at the University of Lausanne; instrumental conditions were accelerating voltage from 12 to 15 kV, beam current from 25 to 30 nA, and spot size of 10 um

Abbreviations: EGZ = enargite-gold zone, EZ = enargite zone, BZ = bornite zone, TZ = tennantite zone, CHZ = chalcoyprite zone, SGZ = sphalerite-galena zone. n.d. = no detected, n.a. = not analyzed

TABLE A2. Additional Microprobe Results Obtained for Some Common and Accessory Phases from the Main Ore Stage, Enargite-Gold Zone

Label	S (wt%)	Fe (wt%)	Cu (wt%)	Zn (wt%)	As (wt%)	Ag (wt%)	Sn (wt%)	Sb (wt%)	Bi (wt%)	Cd (wt%)	V (wt%)	Au (wt%)	Te (wt%)	Total
Enargite														
PBR-132	32.55	0.25	48.49	n.d.	17.33	n.d.	0.16	0.45	0.18	0.01	n.d	0.11	n.d	99.54
PBR-132	31.97	0.14	47.78	0.11	15.99	n.d.	1.61	1.16	n.d.	0.01	n.d	0.20	n.d	98.97
PBR-263	32.89	0.05	48.66	0.04	16.80	0.31	0.30	0.74	n.d.	n.d	n.d.	n.d	n.d	99.79
PBR-263	33.36	n.d.	48.88	0.28	17.32	0.09	0.67	0.26	n.d.	n.d	n.d.	n.d	n.d	100.86
PBR-263	33.18	0.05	48.36	n.d.	17.11	0.10	0.34	0.40	0.25	n.d	n.d.	n.d	n.d	99.79
PBR-263	33.08	0.01	49.02	n.d.	17.11	0.03	0.23	0.89	n.d.	n.d	n.d.	n.d	n.d	100.37
PBR-263	32.98	n.d.	49.22	0.03	17.07	0.03	0.26	0.83	n.d.	n.d	0.02	n.d	n.d	100.44
PBR-137	32.77	0.03	48.59	0.13	17.01	0.09	0.43	0.81	n.d.	n.d	n.d.	n.d	n.d	99.85
PBR-137	32.53	0.08	48.70	0.08	17.00	0.03	0.72	0.54	n.d.	n.d	0.01	n.d	n.d	99.69
PBR-137	30.34	0.01	45.08	0.07	16.05	0.61	6.37	0.21	n.d.	n.d	n.d.	n.d	n.d	98.73
PBR-137	33.19	0.02	48.82	0.04	17.22	0.07	0.27	0.50	n.d.	n.d	n.d.	n.d	n.d	100.13
PBR-137	33.20	0.10	49.27	n.d.	17.67	0.07	n.d.	0.02	n.d.	n.d	n.d.	n.d	n.d	100.33
PBR-137	30.79	0.05	45.35	0.04	18.46	0.09	0.23	0.75	n.d.	n.d	0.02	n.d	n.d	95.78
PBR-137	33.25	0.12	48.66	0.04	17.38	0.11	0.47	0.44	n.d.	n.d	0.02	n.d	n.d	100.49
PBR-137	33.01	0.27	48.73	0.07	17.61	0.05	0.04	0.10	n.d.	n.d	n.d.	n.d	n.d	99.89
PBR-137	33.03	1.09	47.19	0.11	16.37	0.10	0.91	1.24	n.d.	n.d	n.d.	n.d	n.d	100.03
PBR-137	32.81	0.62	47.14	1.11	16.52	0.27	0.37	n.d.	n.d.	n.d	0.07	n.d	n.d	98.91
PBR-132	32.55	0.25	48.49	n.d.	17.33	n.d.	0.16	0.45	0.18	0.01	n.d	0.11	n.d	99.54
PBR-132	31.97	0.14	47.78	0.11	15.99	n.d.	1.61	1.16	n.d.	0.01	n.d	0.20	n.d	98.97
PBR-143	31.73	0.09	49.57	n.d	16.89	n.d.	0.16	0.30	n.d.	0.01	n.d	n.d.	n.d	98.75
PBR-143	24.02	0.06	66.56	n.d	4.05	0.04	2.10	n.d.	n.d.	n.d.	n.d	0.02	n.d	96.86
PBR-143	31.26	0.40	48.72	n.d	17.00	0.03	0.21	0.17	n.d.	n.d.	n.d	n.d.	n.d	97.79
Hessite														
PBR-263	0.05	0.03	0.79	0.02	0.01	60.37	n.d.	0.09	0.03	n.d	0.24	n.d	39.25	100.87
PBR-263	0.03	0.01	0.75	n.d.	n.d.	57.52	n.d.	0.13	n.d.	n.d	n.d.	n.d	42.21	100.64
Luzonite														
PBR-132	29.64	7.00	41.30	2.54	1.13	n.d.	17.19	0.70	n.d.	n.d.	n.d	0.03	n.d	99.55
PBR-132	29.54	7.81	41.39	2.58	0.84	n.d.	16.36	0.83	n.d.	n.d.	n.d	0.08	n.d	99.44
PBR-132	32.61	0.05	48.39	n.d.	17.02	n.d.	0.36	0.86	n.d.	n.d.	n.d	0.11	n.d	99.40
PBR-132	32.61	0.05	48.39	n.d.	17.02	n.d.	0.36	0.86	n.d.	n.d.	n.d	0.11	n.d	99.40
Pyrite														
PBR-132	53.45	46.86	0.82	0.01	0.04	n.d.	0.03	0.03	n.d.	n.d.	n.d	n.d.	n.d	101.22
PBR-137	54.71	45.58	1.31	0.03	0.02	0.04	n.d.	n.d.	n.d.	n.d	n.d.	n.d	n.d	101.67
PBR-137	54.40	46.02	0.32	0.02	0.02	0.01	0.02	0.01	n.d.	n.d	0.02	n.d	n.d	100.82
PBR-137	54.77	45.94	0.41	n.d.	0.04	0.01	0.05	n.d.	n.d.	n.d	0.01	n.d	n.d	101.23
PBR-137	54.85	45.76	0.09	0.02	0.02	n.d.	0.04	n.d.	n.d.	n.d	n.d.	n.d	n.d	100.78
PBR-137	54.68	46.71	0.29	0.02	0.01	0.01	0.04	n.d.	n.d.	n.d	0.01	n.d	n.d	101.75
PBR-132	53.45	46.86	0.82	0.01	0.04	n.d.	0.03	0.03	n.d.	n.d.	n.d	n.d.	n.d	101.22
PBR-143	51.05	46.19	n.d.	n.d.	0.05	0.04	0.07	0.01	n.d.	0.06	n.d	n.d.	n.d	97.46
PBR-143	51.08	44.83	1.84	n.d	0.03	0.03	0.01	n.d.	n.d.	0.12	n.d	n.d.	n.d	97.95
Stannoidite														
PBR-132	29.61	8.35	41.30	2.10	0.99	n.d.	16.83	n.d.	n.d.	0.01	n.d	0.02	n.d	99.20
PBR-132	29.61	8.35	41.30	2.10	0.99	n.d.	16.83	n.d.	n.d.	0.01	n.d	0.02	n.d	99.20
PBR-132	29.64	7.00	41.30	2.54	1.13	n.d.	17.19	0.70	n.d.	n.d.	n.d	0.03	n.d	99.55
PBR-132	29.54	7.81	41.39	2.58	0.84	n.d.	16.36	0.83	n.d.	n.d.	n.d	0.08	n.d	99.44
PBR-263	28.74	8.22	43.62	0.40	1.72	n.d.	14.82	0.89	n.d.	n.d	0.06	n.d	0.04	98.51
PBR-263	28.04	4.17	39.78	1.17	1.43	n.d.	24.11	n.d.	n.d.	n.d	n.d.	n.d	0.06	98.75
Tennantite														
PBR-132	28.44	3.78	44.54	3.51	18.26	0.04	0.41	0.40	n.d.	n.d.	n.d	n.d.	n.d	99.40
PBR-132	30.85	0.59	54.51	0.06	8.10	n.d.	6.55	1.11	n.d.	n.d.	n.d	n.d.	n.d	101.76
PBR-132	28.41	2.53	67.93	0.07	0.03	0.39	0.01	0.02	n.d.	0.05	n.d	0.01	n.d	99.45
PBR-132	28.44	3.78	44.54	3.51	18.26	0.04	0.41	0.40	n.d.	n.d.	n.d	n.d.	n.d	99.40
PBR-263	27.84	6.86	44.35	0.02	18.97	n.d.	0.07	0.17	n.d.	n.d	n.d.	n.d	0.03	98.31
PBR-263	28.99	8.59	42.87	1.09	1.36	n.d.	15.40	n.d.	n.d.	n.d	0.15	n.d	0.01	98.46
Covellite														
PBR-132	28.41	2.53	67.93	0.07	0.03	0.39	0.01	0.02	n.d.	0.05	n.a.	0.01	n.a.	99.45
PBR-132	30.62	0.86	47.37	0.55	8.32	n.d.	7.34	2.13	n.d.	0.02	n.a.	0.12	n.a.	97.33

TABLE A2. *(Cont.)*

Label	S (wt%)	Fe (wt%)	Cu (wt%)	Zn (wt%)	As (wt%)	Ag (wt%)	Sn (wt%)	Sb (wt%)	Bi (wt%)	Cd (wt%)	V (wt%)	Au (wt%)	Te (wt%)	Total
Stutzite														
PBR-263	0.05	0.03	0.79	0.02	0.01	60.37	n.d.	0.09	0.03	n.a.	0.24	n.a.	39.25	100.87
PBR-263	0.03	0.01	0.75	n.d.	n.d.	57.52	n.d.	0.13	n.d.	n.a.	n.d.	n.a.	42.21	100.64
Goldfieldite														
PBR263	25.70	0.04	45.90	n.d.	5.52	0.08	0.05	1.52	0.03	n.a.	n.a.	n.a.	19.90	98.74
PBR263	25.70	0.04	45.90	n.d.	5.52	0.08	0.05	1.52	0.03	n.a.	n.a.	n.a.	20.90	99.74
Kostovite														
PBR263	0.05	n.a.	8.38	n.a.	n.d.	3.35	n.d.	0.24	n.a.	n.a.	n.a.	24.68	65.81	102.51
PBR263	n.d.	n.a.	8.40	n.a.	n.d.	0.52	n.d.	0.28	n.a.	n.a.	n.a.	25.06	67.23	101.49
Native tellurium														
PBR263	n.d.	n.d.	n.d.	n.d.	n.d.	n.d.	n.d.	0.42	n.d.	n.d.	n.d.	0.17	101.59	102.18

A complete list of results are available in Bendezú (2007)

Sulfides were analyzed using a Cameca SX50 electron microprobe at the University of Lausanne; instrumental conditions were accelerating voltage of 12 kV, beam current of 30 nA, and spot size of 10 mm

n.d. = not detected, n.a. = not analyzed

TABLE A3. Composition of Electrum Grains in Three Samples from the Enargite-Gold Zone

Muestra	Au	Ag	Cu	Cd	Zn	Fe	S	Total
PBR-132	81.32	16.21	2.17	0.57	0.06	0.11	0.09	100.53
PBR-132	82.04	16.44	1.89	0.49	0.09	0.19	0.11	101.26
PBR-132	80.67	15.88	3.23	0.42	0.46	0.12	0.08	100.85
PBR-132	82.70	16.01	1.21	0.50	0.02	0.16	0.13	100.73
PBR-245	83.05	15.33	2.94	0.23	0.03	0.14	0.13	101.85
PBR-245	82.28	15.49	2.43	0.21	0.03	0.03	0.05	100.52
PBR-245	81.79	15.40	2.42	0.21	0.03	0.03	0.05	99.92
PBR-265	81.30	15.30	2.40	0.21	0.03	0.03	0.05	99.32

Minerals were analyzed using a Cameca SX50 electron microprobe at the University of Lausanne; instrumental conditions were: accelerating voltage of 12 kV, beam current of 30 nA, and spot size of 10 mm

TABLE A4. Additional Microprobe Results Obtained for Some Common Phases from the Bornite, Tennantite, and Chalcopyrite Zones

Sample no.	Mineral	Zone	S	Fe	Cu	As	Ag	Sb	Bi	Sn	Zn	Total
PBR-187	Bornite	Bornite	25.37	11.18	64.06	0.03	0.01	0.02	n.a.	0.11	n.a.	99.82
PBR-187	Bornite	Bornite	25.89	11.21	64.87	0.07	0.01	0.02	n.a.	0.14	n.a.	99.82
PBR-187	Bornite	Bornite	25.26	11.20	64.65	0.03	0.12	0.05	n.a.	0.04	n.a.	99.82
PBR-95	Tennantite	Tennantite	28.22	3.33	46.13	18.77	0.01	0.83	0.00	0.15	3.91	101.34
PBR-95	Tennantite	Tennantite	28.38	7.02	46.57	19.47	0.00	0.06	0.00	0.00	0.02	101.53
PBR-95	Tennantite	Tennantite	28.44	3.78	44.54	18.26	0.04	0.40	0.00	0.41	3.51	99.40
PBR-123	Chalcopyrite	Chalcopyrite	34.63	29.50	34.74	0.03	0.06	0.07	0.09	0.03	0.00	99.15
PBR-123	Chalcopyrite	Chalcopyrite	34.37	29.93	34.65	0.01	0.00	0.00	0.00	0.06	0.14	99.17
PBR-123	Chalcopyrite	Chalcopyrite	34.44	29.43	34.56	0.02	0.03	0.05	0.00	0.06	0.32	98.91

Notes: Sulfides were analyzed using a Cameca SX50 electron microprobe at the University of Lausanne; instrumental conditions were accelerating voltage of 12 kV, beam current of 30 nA, and spot size of 10 mm

TABLE A5. List of Samples Studied in This Work

Sample no.	Deposit/area	Macroscopic description	Type of analysis																
			XRD	XRF	ICP	NA	MP	REE	CY	TS	PS	S	C	O	H	Pb	Sr	Dat	F I
PBR 50	Colquijirca	Massive sulfide replacement in moderately silicified dolostone py (15 vol %), sl (10 vol %), ga (8 vol %), kao (5 vol %)																	
PBR-54	Smelter	Massive sulfide replacement 30 vol % pyrite, 35 vol % enargite, and 25 vol % quartz; minor tiny alunite grains																	
PBR-55	Smelter	Breccia dolostone clasts (40 vol %) in calcareous matrix (40 vol %) with some pyrite and sphalerite (5 vol % of each)																	
PBR-56	Smelter	Massive sulfide replacement 30 vol % pyrite, 30 vol % enargite, 30 vol % quartz, 10 vol % alunite																	
PBR-57	Smelter	Breccia dolostone clasts (30 vol %) in calcareous matrix (60 vol %); 5 vol % of disseminated pyrite																	
PBR-58	Smelter	Argillaceous rock with relict dolostone; 20 vol % pyrite replacement																	
PBR-59	Colquijirca	Strongly oxidized mineralized dolostone; some relict galena is present (2 vol %)																	
PBR-60	Colquijirca	Massive sulfide replacement in former dolostone; 5 vol % ga, 5 vol % py, 2 vol % sl, 2 vol % kao, 10 vol % sid																	
PBR-61a	Colquijirca	Bituminous mudstone galena (10 vol %) and kaolinite (5 vol %) in fractures and along stratification																	
PBR 61b	Colquijirca	Massive sulfide replacement; 10 vol % galena, 25 vol % pyrite, 25 vol % sphalerite, 5 vol % falhore, 5 vol % kaolinite																	
PBR-62	Colquijirca	Massive sulfide replacement in former dolostone; 50 vol % galena, 20 vol % chalcopyrite, 15 vol % kaolinite, 8 vol % quartz																	
PBR-63	Colquijirca	Massive sulfide replacement in former dolostone; 60 vol % galena, 25 vol % pyrite, 10 vol % kaolinite																	
PBR-64	Smelter	Highly mineralized and altered porphyrytic volcanic rock; pyrite-rich "vuggy quartz" 15 vol % alunite,10 vol % pyrophyllite?																	
PBR-94	Colquijirca	Bi-rich ore massive sulfide replacement in former dolostone; variable amounts of sl, ga, cpy, py, qtz, kao, dick, ba, hm																	
PBR-95	Colquijirca	Bi-rich ore massive sulfide replacement in former dolostone; variable amounts of sl, ga, cpy, py, qtz, kao, dick, ba, hm																	
PBR-96	Colquijirca	Bi-rich ore massive sulfide replacement in former dolostone; variable amounts of sl, ga, cpy, py, qtz, kao, dick, ba, hm																	
PBR-97	Colquijirca	Bi-rich ore massive sulfide replacement in former dolostone; variable amounts of sl, ga, cpy, py, qtz, kao, dick, ba, hm																	
PBR-98	Colquijirca	Silver-rich? sphalerite concentrate FPE-135																	
PBR-99	Colquijirca	Silver-rich? sphalerite concentrate FPE-136																	
PBR-100	Smelter	Enargite-pyrite massive replacement in silicified dolostone																	
PBR-101	Colquijirca	Dolostone with sphalerite-pyrite-galena-enargite partial replacements (together 20 vol %)																	
PBR-101b	Colquijirca	Galena-sphalerite-pyrite massive replacement in former dolostone asociated with argillic alteration																	
PBR-102	Colquijirca	Silicified dolostone, lixiviation cavities coated by pyrite-enargite																	
PBR-103	Colquijirca	Pyrite-chalcopyrite-barite-quartz-sphalerite massive replacement in former dolostone																	
PBR-104	Marcapunta Este	Galena-sphalerite massive replacement in dacitic?; volcanic rock associated with advanced argillic alteration																	
PBR-105	Smelter	Pyrite-galena-sphalerite massive replacement in former dolostone associated with advanced argillic alteration																	
PBR-106	Marcapunta Sur	Enargite-pyrite massive replacements in silicified dolostone																	
PBR-107	Colquijirca	Dolostone with galena-sphalerite in "open-space filling" textures																	
PBR-108	Colquijirca	Cherty breccia with galena-sphalerite-alunite replacing matrix																	

TABLE A5. *(Cont.)*

Sample no.	Deposit/area	Macroscopic description	Type of analysis																	
			XRD	XRF	ICP	NA	MP	REE	CY	TS	PS	S	C	O	H	Pb	Sr	Dat	F	I
PBR-109	Colquijirca	Marcasite?-pyrite?-sphalerite in banded textures; protore: dolostone																		
PBR-110	Colquijirca	Black shale cut by micrometric thick veinlets of galena																		
PBR-111	Colquijirca	Galena-pyrite-barite massive replacement associated with argillic alteration																		
PBR-112	Colquijirca	Massive dickite-kaolinite replacement in former dolostone; minor disseminations of sphalerite and pyrite																		
PBR-113	Colquijirca	Massive galena-sphalerite-pyrite replacement in former dolostone; moderate silicification																		
PBR-114	Colquijirca	Cherty rock with pyrite disseminations and alunite-kaolinite in fractures																		
PBR-115	Colquijirca	Galena, pyrite, sphalerite massive replacement in thin-bedded dolostone; kaolinite in "septarian filling"																		
PBR-116	Colquijirca	Massive galena-pyrite-kaolinite assemblage replacing dolostone																		
PBR-117	Colquijirca	Silicified dolostone partly replaced by euhedral barite-enargite grains																		
PBR-118	Colquijirca	Galena-pyrite-barite massive replacement in former dolostone																		
PBR-119	Colquijirca	Massive argillic alteration minerals; dickite-kaolinite main constituents																		
PBR-120	Colquijirca	Dolostone with dissolution cavities filled with sphalerite-pyrite-barite																		
PBR-121	Colquijirca	Pyrite-sphalerite-barite replacements along bedding and as open-space filling textures																		
PBR-122	Colquijirca	Cherty breccia with pyrite-galena-kaolinite replacing the matrix																		
PBR-123	Colquijirca	Fine-grained subhedral to euhedral pyrite-sphalerite-galena-chalcopyrite as disseminations in massive, kaolinite-rich rock																		
PBR-124	Colquijirca	Argillite with massive galena replacement; remnant of fossils?																		
PBR-125	Colquijirca	Cherty breccia with enargite-pyrite-quartz in geodes																		
PBR-127	Smelter	Recrystallized dolostone with minor sphalerite-pyrite in cavities																		
PBR-128	Smelter	Oxidized fine-grained Miti Group sandstone flow? structures in Mitu red beds?																		
PBR-129	Smelter	Fine-grained pyrite disseminations; minor pyrite replacement in former dolostone																		
PBR-130	Smelter	Breccia chert clasts with pyrite-kaolinite-alunite replacing the matrix; minor sphalerite and zunyite																		
PBR-131	Smelter	Pyrite-enargite massive replacement in former dolostone; coarse-grained alunite in open spaces																		
PBR-132	Smelter	Enargite massive replacement in former dolostone; according to mine analysis >5 g/t Au																		
PBR-132b	Smelter	Strongly silicified dolostone; some portions containing nearly euhedral grains																		
PBR-133	Smelter	Nearly euhedral grains of pyrite and enargite replacing silicfied dolostone																		
PBR-134	Smelter	Mineralized Mitu Group sandstone enargite-pyrite-kaolinite as thin veins minor sphalerite, galena and pyrite																		
PBR-135	Smelter	Enargite-pyrite massive replacement in former dolostone; subordinate enargite-quartz in "cockade" textures																		
PBR-136	Smelter	Sphalerite-galena-pyrite replacement in dacitic volcanic rock (mainly replacing feldspars grains)																		
PBR-137	Smelter	Silicified dolostone containing pink, coarse-grained alunite in geodes																		
PBR-138	Smelter	Dolostone partly silicied with pyrite-enargite in tiny spaces																		
PBR-139	Smelter	Pyrite-enargite-quartz massive replacement in former dolostone																		

TABLE A5. *(Cont.)*

Sample no.	Deposit/area	Macroscopic description	Type of analysis																	
			XRD	XRF	ICP	NA	MP	REE	CY	TS	PS	S	C	O	H	Pb	Sr	Dat	F	I
PBR-140	Smelter	Slightly mineralized dolostone; tiny cavities containing well-formed enargite grains								■	■									
PBR-141	Smelter	Slightly mineralized fine-grained sandstone?; minor pyrite-enargite replacement according to mine analysis >3 g/t Au								■	■									
PBR-143	Smelter	Vuggy silica; vugs partially filled by enargite-pyrite-quartz assemblages			■	■	■				■			■						
PBR-143b	Smelter	Strongly silicified sandstone (Mitu Group); enargite and minor amounts of pyrite as veins or as replacements along bedding			■	■	■			■	■									
PBR-144	Smelter	Massive quartz-chalcopyrite-pyrite-enargite replacement in former dolostone (strong silicified)		■	■	■														
PBR-145	Smelter	Dacitic volcanic rock; moderately chloritized								■										
PBR-146	Smelter	Dolostone displaying enargite-pyrite-alunite replacement along bedding								■	■									
PBR-147	Smelter	Nearly massive sphalerite-siderite-enargite-pyrite replacement in former dolostone; minor kaolinite filling intergranular spaces		■										■	■					
PBR-148	Smelter	Unaltered? biotite-rich dacitic volcanic rock		■				■		■								■		
PBR-149	Smelter	Mitu Group sandstone showing slight reaction to HCl (minor amounts of calcite?)								■										
PBR-150	Smelter	Sphalerite-siderite-enargite; massive replacement in former dolostone; minor kaolinite filling intergranular spaces		■						■	■									
PBR-151	Colquijirca	Chalcopyrite-supported breccia with minor barite and kaolinite; clasts of strongly silicified limestones												■	■					
PBR-152	Smelter	Breccia pyrite-enargite-kaolinite replacing the matrix		■						■										
PBR-180	Colquijirca	Mitu Group argillite														■				
PBR-184	San Gregorio	Strongly oxidized rock presumably containing Bi-bearing oxides; protore: Pucara limestones		■	■	■														
PBR-185c	San Gregorio	Unaltered? biotite-rich dacitic volcanic rock		■				■												
PBR-186	San Gregorio	Strongly oxidized rock presumably containing Bi-bearing oxides; protore: Pucara limestones		■	■															
PBR-187	San Gregorio	Strongly oxidized rock presumably containing Bi-bearing oxides; protore: Pucara limestones		■			■				■									
PBR-188	Colquijirca	Cherty rock alunite-pyrite in fractures								■										
PBR-189	Colquijirca	Black cherty rock; alunite-pyrite in fractures								■										
PBR-190	Colquijirca	Cherty breccia; tennantite-barite replacing the matrix		■	■	■	■				■									
PBR-191	Colquijirca	Massive ore replacement in former dolostone; minor tennantite is the only observed mineral									■									
PBR-192	Colquijirca	Massive ore replacement dickite in speckled textures accompanied by minor pyrite and enargite disseminations												■	■					
PBR-193	Colquijirca	Massive sphalerite-galena replacement ore unrecognized fine-grained green grains, possibly uranium minerals		■	■	■	■				■	■								
PBR-194	Smelter	Dacitic lava-dome affected by advanced argillic alteration (quartz-alunite-bearing assemblages)								■										
PBR-195	Smelter	Dacitic lava-dome affected by advanced argillic alteration (aquartz-alunite-bearing assemblages)								■										
PBR-196	Smelter	Dacite displaying moderate argillic alteration; minor pyrite disseminations			■					■										
PBR-197	Marcapunta	"Vuggy silica"; small (<.05 cm long) subhedral to euhedral quartz grains		■	■	■				■	■									

TABLE A5. *(Cont.)*

Sample no.	Deposit/area	Macroscopic description	Type of analysis																	
			XRD	XRF	ICP	NA	MP	REE	CY	TS	PS	S	C	O	H	Pb	Sr	Dat	F	I
PBR-198	Oro Marcapunta	Dacite displaying advanced argillic alteration; quartz-alunite replacing mainly K feldspars			■	■				■		■		■	■			■		
PBR-199	Smelter	Dacite with no discernable hydrothermal alteration		■				■		■										
PBR-200	Smelter	Dacite slightly altered presence of smectite, according to PIMA II																		
PBR-201	Smelter	Dacite slightly altered presence of smectite, according to PIMA II																		
PBR-202	Smelter	Dacite affected by advanced argillic alteration; quartz-alunite > 50 vol % replacing mainly K feldspars								■										
PBR-203	Smelter	Unoxidated "vuggy silica"; minor pyrite disseminations			■					■	■					■				
PBR-204	Smelter	Strongly kaolinized dacite								■										
PBR-205	Smelter	Massive pyrite-enargite-alunite replacement in dacite								■	■									
PBR-206	Colquijirca	Excelsior Group phyllite														■				
PBR-217	Colquijirca	Chert-alunite-enargite-pyrite; semimassive replacement in former dolostone; sulfides and alunite mainly in fractures			■	■								■	■					
PBR-218	Colquijirca	Chert-alunite-enargite-pyrite; semimassive replacement in former dolostone; sulfides and alunite mainly in fractures			■	■	■			■	■			■	■			■		
PBR-230	Colquijirca	Massive chert-pyrite-enargite and kaolinite in cavities									■			■	■					
PBR-234	Smelter	Massive enargite-pyrite ore accompanied by minor quartz		■	■	■	■													
PBR-238	Smelter	Pyrite-enargite-alunite in geodes, replacing clasts in sedimentary breccia					■			■				■	■					
PBR-240	Colquijirca	Strongly argillized ore pyrite-galena-sphalerite-chalcopyrite in botroidal aggregates and coarse disseminations		■							■			■	■					
PBR-241	Colquijirca	Strongly argillized ore pyrite-galena-sphalerite-barite in geode-like pockets					■				■			■	■					
PBR-244	Colquijirca	Pyrite-supported breccia; minor enargite-alunite-dickite? as accompanying minerals		■	■	■	■			■	■	■		■	■			■		
PBR-245	Smelter	Massive enargite in radial aggregates; subordinate pyrite associated with well-formed alunite			■	■	■			■	■			■	■					
PBR-246	Colquijirca	Specular hematite associated with siderite; kaolinite as open-space filling												■	■					
PBR-247	Colquijirca	Galena-sphalerite in a mass of dickite and as open-space filling in chert; in this last case associated with quartz					■				■	■		■	■					
PBR-248	Colquijirca	Galena-chalcopyrite-quartz in porous chert replacing former dolostone									■									
PBR-249	Colquijirca	Massive pyrite-enargite replacement ore; abundant dickite-kaolinite associated with the sulfides					■			■				■	■					
PBR-250	Smelter	Kaolinite in open-space filling textures; sphalerite-galena-barite-hematite? in small geodes in silicified dolostones					■			■				■	■					
PBR-251	Smelter	Monominerallic dickite sample from enargite-pyrite-bearing sample												■	■					
PBR-252	Colquijirca	Siderite-ankerite-sphalerite massive replacement; minor fluorite as well-formed grains								■			■	■	■					
PBR-253	Colquijirca	Massive sphalerite-galena replacement; alunite and barite intimately intergrown with sulfides in vugs		■	■	■	■			■	■	■		■	■					
PBR-255	Smelter	Sphalerite-galena-pyrite-hematite-kaolinite; massive replacement in former dolostone					■				■			■	■					
PBR-256	Smelter	Massive enargite-pyrite replacement in conglomeratic rock (Shuco member?) minor alunite					■				■									
PBR-259	Smelter	Massive chert-pyrite-enargite-alunite replacement in former dolostone										■								

TABLE A5. *(Cont.)*

Sample no.	Deposit/area	Macroscopic description	Type of analysis																	
			XRD	XRF	ICP	NA	MP	REE	CY	TS	PS	S	C	O	H	Pb	Sr	Dat	F	I
PBR-260	Smelter	Massive sphalerite-galena-siderite/ankerite replacement in former dolostone																		
PBR-262	Smelter	Enargite-pyrite-alunite as open space filling from semimassive ore																		
PBR-263	Smelter	Massive enargite-pyrite-quartz-alunite-dickite replacement; some chert clasts																		
PBR-265	Smelter	Massive enargite-pyrite-alunite-quartz replacement besides relict chert																		
PBR-266	Marcapunta	Alunite replacing matrix in dacite																		
PBR-267	Smelter	Massive enargite-pyrite-chalcopyrite replacement minor alunite-kaolinite?																		
PBR-269	Smelter	Massive enargite-alunite replacement in former dolostone																		
PBR-270	Smelter	Massive pyrite-enargite-chalcopyrite?-sphalerite-galena? Replacement in former dolostone																		
PBR-272	Smelter	Strongly altered dacite; alunite replacing groundmass																		
PBR-277	Colquijirca	Strongly silicified dolostone; abundant siderite accompanied by minor galena and sphalerite																		
PBR-281	San Gregorio	Sulfide-rich silicified ore; only fine-grained pyrite visible																		
PBR-282	Colquijirca	Massive sphalerite-galena-chalcopyrite replacement in former dolostone																		
PBR-283	Colquijirca	Quartz sample from bornite-rich zone																		
PBR-286	Colquijirca	Massive sulfide replacement; mainly pyrite, bornite, minor quartz																		
PBR-288	Colquijirca	Massive enargite-pyrite replacement associated with fine-grained alunite																		
PBR-290	Colquijirca	Massive enargite-pyrite replacement associated with fine-grained alunite																		
PBR-291	Colquijirca	Sulfide-rich ore; mainly pyrite and bornite associated with well-formed quartz																		
PBR-298	Colquijirca	Massive sphalerite, pyrite, galena replacement; centimetric geodes coated by alunite euhedral grains																		
PBR-305	Oro Marcapunta	Vuggy silica; vugs partially filled by botryoidal hematite and quartz																		
PBR-310	Colquijirca	Semimassive sulfide replacement; chacopyrite-pyrite association accompanied by quartz																		
PBR-311	Colquijirca	Mineralized breccia; strongly silicified angular clasts in a matrix dominated by kaolinite																		
PBR-312	Colquijirca	Mineralized breccia; chert angular clasts in a chalcopyrite-rich matrix; minor kaolinite filling cavities																		
PBR-313	Colquijirca	Massive galena replacement; siderite as spherical aggregates																		
PBR-314	Smelter	Massive enargite-luzonite-pyrite replacement																		
PBR-321	Smelter	Massive pyrite-enargite replacement in strongly silicified conglomerate (Shuco member?); two pyrite generations																		
PBR-322	Smelter	Mineralized breccia matrix partially replaced by enargite and coarse-grained alunite																		
PBR-324	Colquijirca	Massive tennantite, chalcopyrite, pyrite replacement associated with argillic alteration (kaolinite?)																		
PBR-325	Colquijirca	Massive tennantite and pyrite replacement associated with coarse grains of barite																		
PBR-326	Colquijirca	Massive pyrite and bornite replacement associated with argillic alteration (dickite?)																		

TABLE A5. *(Cont.)*

Sample no.	Deposit/area	Macroscopic description	Type of analysis																	
			XRD	XRF	ICP	NA	MP	REE	CY	TS	PS	S	C	O	H	Pb	Sr	Dat	F	I
PBR-327	Smelter	Massive enargite-pyrite replacement in former carbonate rock; large acicular aggregates of enargite		■	■	■					■									
PBR-329	Smelter	Nearly massive ore replacement; coarse euhedral enargite; alunite postdating enargite as coatings around pyrite					■			■				■	■					
PBR-332	Smelter	Massive pyrite-enargite replacement in former dolostone two pyrite generations; aunite as open-space filling		■	■	■														
PBR-391	Smelter	Massive quartz-pyrite replacement in carbonate-rocks; coarse-grained quartz in geodes		■	■	■								■						
PBR-398	Colquijirca	Massive siderite (and other unidentified carbonates) as botryoidal aggregates in open spaces		■	■	■														
PBR-399a	Colquijirca	Massive sphalerite-galena replacement; subordinate hematite and siderite plus minor kaolinite	■				■				■									
PBR-399b	Smelter	Strongly silicified rock; limestone with pyrite and quartz mainly as disseminations and veinlets; opaline silica accompanying quartz		■	■	■								■						
PBR-400	Colquijirca	Native silver overgrowing euhedral to subhedral galena-sphalerite aggregates					■				■									

Notes: The table includes details such a macroscopic description and the type of analysis conducted;

Field work consisted mainly of logging and revising correlations of nearly 25,000 m of core drilled along a north-south longitudinal section through the system, and three selected east-west transverse sections; mapping of selected parts of the open pits in the Colquijirca deposit was also undertaken; in addition, the present study integrates information accumulated by the geological staff at Colquijirca as well as numerous personal communications with the other mine geologists; laboratory workconsisted of the study of 257 representative samples from throughout the Smelter-Colquijirca corridor—of these, 154 thin and/or polished sections were studied by microscopy and many by X-ray diffraction, infrared microscopy, electron microprobe (analyses in Appendix 1), Raman spectroscopy and scanning electron microscopy; locations of the studied samples as well as the analytical techniques used are given in Appendix 2

TABLE A6. Sample Locations

Sample no.	Hole		Location: Depth	Location: Area	UTM Coordinates: E	UTM Coordinates: N
PBR- 50	S.D. # 3		39.7	Colquijirca	360967	8811762
PBR-54	BR.-524		548.5	Marcapunta	361090	8808563
PBR-55	CM8-580		201.9	Smelter	361588	8809263
PBR-56	CM5-580		101.5	Smelter	361190	8809262
PBR-57	CM1-580		159.6	Smelter	360690	8809262
PBR-58	SM2-644		199.5	Smelter	361172	8810074
PBR-59	TN7-724		119.5	Colquijirca	361785	8811066
PBR-60	TN2-728		159.5	Colquijirca	361221	8811115
PBR-61a		Open pit		Colquijirca		
PBR-61b		Open pit		Colquijirca		
PBR-62		Open pit		Colquijirca		
PBR-63	TN3-776		92.9	Colquijirca	361199	8811712
PBR-64	CM2-548		243.8	Smelter	360689	8808863
PBR- 94		Mercedes Norte pit		Colquijirca		
PBR- 95		Mercedes Norte pit		Colquijirca		
PBR- 96		Mercedes Norte pit		Colquijirca		
PBR- 97		Mercedes Norte pit		Colquijirca		
PBR- 98		Mercedes Norte pit		Colquijirca		
PBR- 99		Mercedes Norte pit		Colquijirca		
PBR-100		Underground adit		Smelter		
PBR-101	SP2-98		195.5	Colquijirca sur	361218	8810162
PBR-101b	SP2-98		209.0	Colquijirca sur	361218	8810162
PBR-102		Principal pit		Colquijirca		
PBR-103	SP2-130		187.5	Colquijirca sur	361251	8810563
PBR-104	CME2-468		152.8	Marcapunta este		
PBR-105	CM13-564		260.5	Smelter este	361987	8809065
PBR-106	DDH7		236.4	Marcapunta sur		
PBR-107	SP2-146		183.5	Colquijirca sur	361271	8810762
PBR-108		Principal pit		Colquijirca	360915	8811135
PBR-109		Principal pit		Colquijirca		
PBR-110		Principal pit		Colquijirca		
PBR-111		Principal pit		Colquijirca		
PBR-112		Principal pit		Colquijirca		
PBR-113		Principal pit		Colquijirca		
PBR-114		Principal pit		Colquijirca		
PBR-115		Principal pit		Colquijirca		
PBR-116		Principal pit		Colquijirca		
PBR-117		Principal pit		Colquijirca		
PBR-118		Principal pit		Colquijirca		
PBR-119		Principal pit		Colquijirca		
PBR-120		Principal pit		Colquijirca		
PBR-121		Principal pit		Colquijirca		
PBR-122		Principal pit		Colquijirca		
PBR-123		Principal pit		Colquijirca		
PBR-124		Principal pit		Colquijirca		
PBR-125		Principal pit		Colquijirca		
PBR-128	CM5-580		265.0	Smelter	361190	8809262
PBR-129	CM5-596		148.8	Smelter	361189	8809262
PBR-130	CM5-580		189.2	Smelter	361190	8809262
PBR-131	CM9-548		247.3	Smelter	361184	8808858
PBR-132	CM6-580		104.2	Smelter	361391	8809263
PBR-132b	CM6-580		116.4	Smelter	361391	8809263
PBR-133		Underground adit		Smelter		
PBR-134	CM7-564		241.5	Smelter	361191	8809062
PBR-135	CM9-548		259.0	Smelter	361184	8808858
PBR-136	CME2-468		355.4	Smelter		
PBR-137	CM5-580		110.4	Smelter	361190	8809262
PBR-138	CM5-596		53.3	Smelter	361189	8809262
PBR-139	CM5-596		140.4	Smelter	361189	8809262
PBR-140	CM10-564		316.3	Smelter	361590	8809064
PBR-141	CM4-564		351.6	Smelter	360890	8809063
PBR-143	Brocal-524		552.9	Smelter	361090	8808563
PBR-143b	Brocal-524		733.0	Smelter	361090	8808563
PBR-144		Underground adit		Smelter		
PBR-145	CM5-580		285.5	Smelter	361190	8809262
PBR-146		Underground adit		Smelter		
PBR-147	CM7-564		266.0	Smelter	361191	8809062

TABLE A6. *(Cont.)*

			Location		UTM Coordinates	
Sample no.	Hole		Depth	Area	E	N
PBR-148	CM13-564		39.0	Smelter	361987	8809065
PBR-148b		Underground adit		Smelter		
PBR-149	CM10-564			Smelter	361590	8809064
PBR-150	CM5-580		262.5	Smelter	361190	8809262
PBR-151	CM11-572		211.9	Smelter	361884	8809178
PBR-152	MB-6		103.7	Smelter	361241	8809899
PBR-180		Outcrop		Colquijirca		
PBR-184		Outcrop		San Gregorio		
PBR-185C		Outcrop		San Gregorio		
PBR-186		Outcrop		San Gregorio		
PBR-187		Outcrop		San Gregorio		
PBR-188		Principal pit		Colquijirca		
PBR-189		Principal pit		Colquijirca		
PBR-190		Principal pit		Colquijirca		
PBR-191		Principal pit		Colquijirca		
PBR-192		Principal pit		Colquijirca		
PBR-193		Principal pit		Colquijirca		
PBR-194	CM10-548		201.8	Smelter	361290	8808863
PBR-195	CME2-468		329.4	Smelter		
PBR-196	CM8-548		168.9	Smelter	361615	8808862
PBR-197	SD-11		144.0	Oro Marcapunta	361128	8808206
PBR-198		Outcrop		Oro Marcapunta	360850	8808526
PBR-199	CM6-548		230.4	Cobre Marcapunta	361389	8808860
PBR-200	CM9-548		66.2	Cobre Marcapunta	361184	8808858
PBR-201	CM9-548		196.0	Cobre Marcapunta	361184	8808858
PBR-202	CM10-548		214.8	Cobre Marcapunta	361290	8808863
PBR-203	CM10-548		191.3	Cobre Marcapunta	361290	8808863
PBR-204	CM2-468		80.0	Cobre Marcapunta	360440	8807863
PBR-205	CM8-564		126.7	Cobre Marcapunta	361291	8809063
PBR-206		Outcrop		Colquijirca		
PBR-217		Principal pit		Colquijirca		
PBR-230		Principal pit		Colquijirca		
PBR-234	CM7-572		196.5	Smelter	361291	8809164
PBR-238	CM6-572		170.2	Smelter	361190	8809162
PBR-240		Principal pit		Colquijirca		
PBR-241		Principal pit		Colquijirca		
PBR-244		Principal pit		Colquijirca	360973	8811061
PBR-245		Underground adit		Smelter		
PBR-246		Choccayoc pit		Colquijirca		
PBR-247		Choccayoc pit		Colquijirca		
PBR-248		Principal pit		Colquijirca		
PBR-249		Principal pit		Colquijirca		
PBR-250		Principal pit		Colquijirca		
PBR-251		Choccayoc pit		Colquijirca		
PBR-252		Choccayoc pit		Colquijirca		
PBR-253		Principal pit		Colquijirca		
PBR-255	CM8-580		205.7	Smelter	361588	8809263
PBR-256	CM5-580		177.5	Smelter	361190	8809262
PBR-259	SM1-676		81.3	Smelter	360920	8810463
PBR-260	MB-13		218.4	Smelter	360857	8809302
PBR-262	MB-7		287.5	Smelter	361200	8808950
PBR-263	CM4-588		160.2	Smelter	361190	8809362
PBR-265	CM7-565		112.9	Smelter		
PBR-266	CM6-572		97.1	Smelter	361190	8809162
PBR-267	SM2-676		137.5	Smelter	361030	8810458
PBR-269	CM6-572		119.8	Smelter	361190	8809162
PBR-270	SM1-676		104.7	Smelter	360920	8810463
PBR-272	CM7-564		109.5	Smelter	361191	8809062
PBR-277	SD-66		200.6	Colquijirca	361490	8811800
PBR-281	37G		194.7	San Gregorio		
PBR-282		Mercedes pit		Colquijirca		
PBR-283		Principal pit		Colquijirca		
PBR-290		Principal pit		Colquijirca		
PBR-291		Principal pit		Colquijirca		
PBR-298		Principal pit		Colquijirca	360947	8811058
PBR-305		Outcrop		Oro Marcapunta		
PBR-310		Mercedes pit		Colquijirca		

TABLE A6. *(Cont.)*

Sample no.	Hole		Location		UTM Coordinates	
			Depth	Area	E	N
PBR-311		Mercedes Norte pit		Colquijirca		
PBR-312		Mercedes Norte pit		Colquijirca		
PBR-313		Mercedes Norte pit		Colquijirca		
PBR-314		Underground adit		Smelter		
PBR-321		Underground adit		Smelter		
PBR-322	DDH-37G		148.0	San Gregorio	361189	8809162
PBR-324		Principal pit		Colquijirca		
PBR-325		Principal pit		Colquijirca		
PBR-326		Principal pit		Colquijirca		
PBR-327		Underground adit		Smelter		
PBR-329		Underground adit		Smelter		
PBR-332		Underground adit		Smelter		
PBR-391		Outcrop		Smelter		
PBR-398		Outcrop		Colquijirca		
PBR-399a		Outcrop		Colquijirca		
PBR-399b		Outcrop		Smelter		
PBR-400		Outcrop		Colquijirca		

Approximate coordinates (±20 m) for samples without data may be requested from the author